WIRELESS COMMUNICATIONS AND MOBILE COMPUTING
Wirel. Commun. Mob. Comput. 2001; **1**:221–242 (DOI: 10.1002/wcm.1)

REVIEW

Estimation of Doppler spread and signal strength in mobile communications with applications to handoff and adaptive transmission

Cihan Tepedelenlioğlu*,† Ali Abdi,
Georgios B. Giannakis and Mostafa Kaveh

200 Union St. SE, Department of
Electronic and Computer Engineering
University of Minnesota
Minneapolis
MN 55455
U.S.A.

Summary

Estimation of signal strength, a measure of channel quality, and Doppler spread which is proportional to the mobile speed, are important for handoff algorithms and optimal tuning of system parameters to changing channel conditions in adaptive transmission systems. This paper provides a survey of existing techniques for estimating the statistical parameters of the mobile channel. We discuss the current state of the art in estimation of the received signal strength, mobile velocity, and other related statistical channel parameters, illustrate their performance, and compare existing techniques. The sensitivity of these schemes to modeling error owing to the presence of line of sight, directional reception, and noise is characterized analytically and illustrated by simulations. Copyright © 2001 John Wiley & Sons, Ltd.

KEY WORDS

Doppler spread
signal strength
mobile velocity

1. Introduction

In mobile communications, the received signal strength fluctuates as the vehicle travels through the interference patterns caused by multipath, shadowing owing to obstructions, and the change in the mobile station (MS)–base station (BS) distance. Statistical characterization of the received signal variations at the MS and estimation of its parameters are instrumental in virtually all aspects of mobile communication system design. For example, handoff initiation decisions are largely based on the mean signal strength that is estimated from the received signal [1–3]. The handoff algorithm parameters such as hysteresis and averaging window size should be chosen to balance the conflicting requirements

*Correspondence to: Cihan Tepedelenlioğlu, 200 Union St. SE, Department of Electronic and Computer Engineering, University of Minnesota, Minneapolis, MN 55455, U.S.A.
†E-mail: cihan@ece.umn.edu

of minimizing handoff delay and mean number of handoffs which depend on the statistical parameters of the received signal.

In many communication applications such as adaptive coding/modulation/antenna diversity/power control, assessing the channel quality and its rate of change is of paramount importance in adapting the system parameters to changing channel conditions [4, 5]. Adaptive transmission systems are designed to maximize their throughput for a given quality of service, usually given in terms of bit error rate (BER). This is possible by adapting the system parameters either to multipath fading fluctuations, or by following the shadow fading variations after removing the deleterious effects of the multipath fading through diversity techniques. In either case, accurate estimation, prediction and tracking of the received signal strength is necessary, which in turn necessitates the estimation of the maximum Doppler spread or its proportional surrogate: the mobile, velocity[‡].

In this paper we give a survey of the existing techniques for estimating the channel quality, measured in terms of the received signal strength, and related parameters such as the maximum Doppler spread, Ricean factor, shadow variance, and shadow correlation distance. After providing a detailed discussion of the signal model and introducing the key channel parameters in Section 2, we give a survey of channel quality estimation techniques in Section 3, with emphasis on local power estimation. The effects of the Ricean factor and other parameters on the local mean estimators are analyzed analytically, and verified via simulation in Section 3.1. After a brief discussion of estimation of the Ricean factor, shadow variance, and shadow correlation distance in Section 3.2, we move on to velocity estimation in Section 4. Level crossing rate (LCR)-based and covariance-based techniques in the literature are discussed in detail, and the effects of noise, modeling errors, and finite data records on the estimators are discussed. In Section 5, we conclude the paper.

A few words on notation: We use* for complex conjugate, $\mathcal{R}\{\cdot\}$ for the real part and $\mathcal{I}\{\cdot\}$ for the imaginary part of a complex number; $E[\cdot]$ denotes mathematical expectation with respect to all the random variables within the brackets; $\delta(t)$ represents Dirac's delta function; superscript $^{(n)}$ denotes nth derivative, but if $n = 1$ or 2, we also use $'$ or $''$, respectively; $\log(\cdot)$ denotes base-10 logarithm and $\ln(\cdot)$ is used for the base e logarithm. For a generic complex, stationary stochastic process $x(t)$, we use $r_x(\tau) := E[x(t)x^*(t+\tau)]$ to denote its correlation function, and reserve $c_x(\tau) := r_x(\tau) - |E[x(t)]|^2$ for the covariance function at lag τ.

2. Signal Model

A widely accepted model for the received power at the mobile station is in the following product form[§]:

$$p(t) = |h(t)|^2 s(t) \tag{1}$$

where $s(t)$ is the power fluctuation due to shadowing, and $h(t)$ is the narrowband channel response due to multipath in complex baseband form. In this paper we will only focus on narrowband channels. Parameter estimation for channels with a nonzero multipath spread is addressed in [6, 7], and references cited therein. The multipath component is commonly assumed to be statistically independent of the shadow process. When the power is measured through a logarithmic amplifier, its decibel (dB) value has the following additive form:

$$P(t) = H(t) + S(t) \tag{2}$$

where $P(t) := 10\log(p(t))$, $S(t) := 10\log(s(t))$, and $H(t) := 10\log(|h(t)|^2)$. The alternative representations of the received power in Equations (1) and (2) are both useful because the multipath fading statistics are more easily described in terms of $h(t)$ in Equation (1), whereas the shadow process is more conveniently characterized statistically by the logarithmic version $S(t)$ in Equation (2). In the following subsections we discuss the statistics of multipath fading and shadow fading in detail.

2.1. Multipath Fading Statistics

In this subsection we discuss the first and second order statistics of $h(t)$, $|h(t)|^2$, $H(t)$ and the level crossing rate of $|h(t)|$ and $h(t)$, which are crucial for design and performance analysis of local power estimators and velocity estimators.

The multipath component $h(t)$ is a result of constructive and destructive superposition of many plane

[‡] We are interested in estimation of the magnitude of the velocity vector, which we loosely refer to as 'velocity' throughout the manuscript.

[§] All the expressions for the received power are given as a function of time and can be equivalently represented in terms of the MS–BS distance d through the MS velocity v by substituting $t = d/v$.

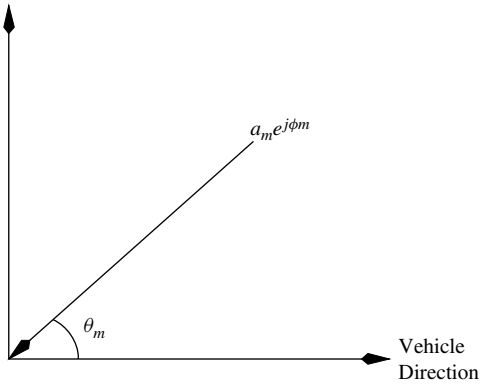

Fig. 1. Contribution of one wave.

waves (see Figure 1) and a possible line of sight (LOS) component. Hence, for a mobile traveling through the interference pattern we adopt the following model for the multipath component in baseband:

$$h(t) = \underbrace{\frac{1}{\sqrt{K+1}} \lim_{M\to\infty} \frac{1}{\sqrt{M}} \sum_{m=1}^{M} a_m e^{j(\omega_D \cos(\theta_m)t+\phi_m)}}_{:=x(t)} + \underbrace{\sqrt{\frac{K}{K+1}} e^{j(\omega_D \cos(\theta_0)t+\phi_0)}}_{:=y(t)} \tag{3}$$

where the maximum Doppler frequency $\omega_D := 2\pi v/\lambda$ is determined by the mobile velocity v and the wavelength λ; $j := \sqrt{-1}$, and M is the number of independent scatterers; the angles between the incoming waves and the mobile antenna θ_m, $m = 1, \ldots, M$ are independent and identically distributed (i.i.d.) with an angle of arrival (AOA) distribution $p(\theta)$; phases ϕ_m are i.i.d., uniformly distributed on $(-\pi, \pi]$; θ_0 and ϕ_0 are the angle that the LOS component makes with the mobile direction and the phase of the LOS component respectively; $K = E|y(t)|^2/E|x(t)|^2$ is the ratio of the LOS component's power to that of the diffuse component and is referred to as the Ricean factor; positive, deterministic constants a_m satisfy $\lim_{M\to\infty} M^{-1} \sum_{m=1}^{M} a_m^2 = 1$, so that the power of the multipath component $E|h(t)|^2$ is normalized to one. We can make this convenient assumption without loss of generality because the product model in Equation (1), along with the independence of $|h(t)|^2$ and $s(t)$, facilitate absorbing the mean value of $p(t)$ into $s(t)$ so that $E[p(t)] = E[s(t)]$.

Note that making M arbitrarily large ensures $x(t)$ to be a complex Gaussian process by the central limit theorem, resulting in a Ricean $|h(t)|$ as the amplitude of a nonzero-mean complex Gaussian process. In the absence of a LOS component ($K = 0$), $|h(t)|$ has a Rayleigh density, and $|h(t)|^2$ is exponentially distributed. Because the phases ϕ_m are uniformly distributed on $(-\pi, \pi]$, $E[x(t)] = 0$ and hence $E[h(t)] = y(t)$. Notice that the specular component $y(t)$ depends on time if the LOS component is not perpendicular to the direction of motion ($\theta_0 \neq \pi/2$); hence, similar to [8] and [9], we allow for a sinusoidally time varying specular component.

It follows from Equation (3) that the correlation function of $h(t)$ is given by

$$\begin{aligned} r_h(\tau) &:= E\left[h(t)h^*(t+\tau)\right] \\ &= \frac{1}{K+1} \int_{-\pi}^{\pi} p(\theta) e^{-j\omega_D \cos(\theta)\tau} d\theta \\ &\quad + \frac{K}{K+1} e^{-j\omega_D \cos(\theta_0)\tau} \end{aligned} \tag{4}$$

by direct substitution and using the assumptions on ϕ_m, θ_m and a_m. We see from Equation (4) that $r_h(\tau)$ depends on the probability distribution of the angle of arrival $p(\theta)$. It is well known that if $p(\theta)$ is uniform and $K = 0$, then $r_h(\tau) = J_0(\omega_D\tau)$, where $J_0(\cdot)$ is the zeroth order Bessel function of the first kind [10]. However, in order to capture the effects of directional scattering on $r_h(\tau)$ in a parametric fashion, we use the von Mises distribution:

$$p(\theta) = \frac{1}{2\pi I_0(\kappa)} e^{\kappa \cos(\theta-\alpha)}, \theta \in (-\pi, \pi] \tag{5}$$

where $I_n(\kappa)$ is the nth order modified Bessel function of the first kind, κ determines the beamwidth, and α denotes the angle between the average scattering direction and the mobile direction. Figure 2 illustrates the von Mises distribution for different values of κ and $\alpha = 0$ in polar coordinates (notice that $\kappa = 0$ reduces Equation (5) to a uniform distribution and that if $\alpha \neq 0$, then the plot rotates by α radians).

The von Mises distribution is widely used in directional statistics [11], and is justified empirically to be an accurate model for the AOA distribution for narrowband channels in [12]. In addition, the von Mises distribution enables us to relate, in closed form, the effect of $\boldsymbol{\psi} := [K, \theta_0, \kappa, \alpha]$ to the Doppler spectrum, the correlation function, and $r_h^{(n)}(0)$ [12].

Substituting Equation (5) into Equation (4) it can be shown [12, 13] that the correlation function is given by:

$$\begin{aligned} r_h(\tau) &= \frac{1}{K+1} \frac{J_0\left(\sqrt{-\kappa^2 + \omega_D^2\tau^2 - 2j\kappa\cos(\alpha)\omega_D\tau}\right)}{I_0(\kappa)} \\ &\quad + \frac{K}{K+1} e^{-j\omega_D \cos(\theta_0)\tau} \end{aligned} \tag{6}$$

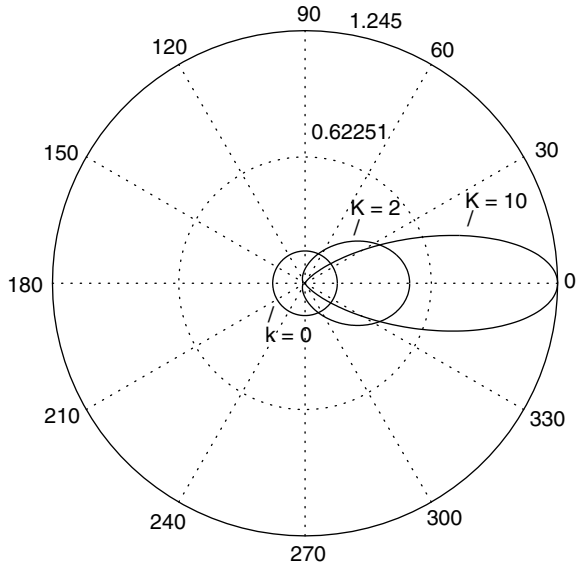

Fig. 2. The von Mises distribution.

Notice that Equation (6) is complex valued in general, but it is real when $K = \kappa = 0$, and reduces to $r_h(\tau) = J_0(\omega_D\tau)$, yielding the so-called Clarke's model [10].

The Doppler spectrum $S_h(\omega)$ is the Fourier transform of Equation (4). Using the fact that $S_h(\omega) = [p(\cos^{-1}(\omega/\omega_D)) + p(-\cos^{-1}(\omega/\omega_D))][1 - (\omega/\omega_D)^2]^{-1/2}$, we obtain a closed-form expression for $S_h(\omega)$ as a function of κ and α:

$$S_h(\omega) = \frac{1}{K+1}\frac{e^{\kappa\cos(\alpha)\frac{\omega}{\omega_D}}\cosh\left[\kappa\sin(\alpha)\sqrt{1-\left(\frac{\omega}{\omega_D}\right)^2}\right]}{\pi I_0(\kappa)\sqrt{1-\left(\frac{\omega}{\omega_D}\right)^2}} + \frac{K}{K+1}\delta(\omega-\omega_D\cos(\theta_0)) \quad (7)$$

where $\cosh(\cdot)$ denotes hyperbolic cosine. Notice that Equation (7) reduces to Clarke's 'U-shaped' spectrum [6] when $\boldsymbol{\psi} = \mathbf{0}$. In this case we have: $S_h(\omega) = \pi^{-1}[1 - (\omega/\omega_D)^2]^{-1/2}$.

The derivatives of the correlation function of the diffuse component at zero, $r_x^{(n)}(0)$, play an important part in estimating the maximum Doppler frequency ω_D. They can be derived for $n = 0, 1, 2$ using Equations (4) and (5) as:

$$r_x(0) = \frac{1}{K+1} \quad (8)$$

$$r_x^{'}(0) = -j\omega_D\frac{1}{K+1}\left(\frac{\cos(\alpha)I_1(\kappa)}{I_0(\kappa)}\right) \quad (9)$$

$$r_x^{''}(0) = -\omega_D^2\frac{1}{2(K+1)}\left(1+\frac{\cos(2\alpha)I_2(\kappa)}{I_0(\kappa)}\right) \quad (10)$$

Equations (8–10) are instrumental in assessing performance of certain velocity (Doppler) estimators in Section 4.

Using the results in Reference [9], it is possible to relate the effects of directional scattering and the LOS component to the envelope level crossing rate (LCR). The LCR of a signal at a level R is defined as the expected number of signal crossings of the level R with positive slope, and can be shown to be (see for example, Reference [2]):

$$\mathrm{LCR}(R) = \int_0^\infty \dot{R}\, p_{|\dot{h}|,|h|}(\dot{R}, R)\, d\dot{R} \quad (11)$$

where $p_{|\dot{h}|,|h|}(\dot{R}, R)$ is the joint probability density function of the envelope and its time derivative. In Reference [9], the authors showed that even in the presence of a specular component and correlated real and imaginary parts of $x(t)$ (which is caused by $\kappa \neq 0$ in our model), the LCR of the envelope is proportional to ω_D and is entirely determined by $r_x^{(n)}(0)$, $n = 0, 1, 2$, given in Equations (8–10):

$$\mathrm{LCR}(R, \psi) = \frac{2R\sqrt{2\beta}}{\pi^{3/2}r_x(0)}e^{-(R^2+\rho^2)/r_x(0)} \times \int_0^{\pi/2}\cosh\left(\frac{2R\rho\cos\theta}{r_x(0)}\right)[e^{-(\xi\rho\sin\theta)} + \sqrt{\pi}\xi\rho\sin\theta\,\mathcal{Q}(\xi\rho\sin\theta)]d\theta \quad (12)$$

where R is the level, $\rho := |y(t)| = [K/(K+1)]^{1/2}$ is the amplitude of the specular component in Equation (3), $\mathcal{Q}(\cdot)$ is the error function, $\beta := -(1/2)r_x^{''}(0) - [\mathcal{I}\{r_x^{'}(0)\}^2/2r_x(0)]$, and $\xi := [\omega_D\cos\theta_0 - \mathcal{I}\{r_x^{'}(0)\}/r_x(0)]/\sqrt{2\beta}$. Equation (12) is a general expression for the envelope level crossing rate and subsumes the well-known formula $\mathrm{LCR}(R,\mathbf{0}) = (\beta/2\pi)^{1/2}(R/r_x(0))\exp[-R^2/(2r_x(0))] = (\omega_D/\sqrt{2\pi})R\exp(-R^2)$ as a special case, commonly used for Doppler estimation through the envelope level crossing estimates [2].

The zero crossing rate of the in-phase or the quadrature-phase (I/Q) components of $h(t)$ (henceforth just ZCR) is also of interest in velocity estimation, and is given by [2]:

$$\mathrm{ZCR}(\boldsymbol{\psi}) = \frac{1}{\pi}\sqrt{\frac{-r_x^{''}(0)}{r_x(0)}}\left[e^{-\zeta}I_0(\eta) + \frac{b^2}{2\zeta}\int_0^\zeta e^{-u}I_0\left(\frac{\eta}{\zeta}u\right)du\right] \quad (13)$$

where $\zeta := (a^2 + b^2)/4$, $\eta := (a^2 - b^2)/4$, $a := \sqrt{2K}$, and $b := \sqrt{2K}\omega_D \cos\theta_0[-r_x(0)/r_x''(0)]^{1/2}$. Using Equations (8) and (10) it is easy to show that b does not depend on ω_D, and hence the ZCR is proportional to the maximum Doppler spread (and hence the velocity). Notice also that while the term inside the brackets in Equation (13) is not defined for $K = 0$, it approaches to one as $K \to 0$. This is not surprising since, it is known that $\mathrm{ZCR}(\mathbf{0}) = \pi^{-1}[-r_x''(0)/r_x(0)]^{1/2}$, which is the term before the brackets in Equation (13).

The model in Equation (3) also enables us to derive the autocovariance of $|h(t)|^2$ as [13]:

$$c_{|h|^2}(\tau) = \frac{1}{(K+1)^2}[|E[e^{j\omega_D \cos(\theta)\tau}]|^2 + 2K\mathcal{R}\{E[e^{-j\omega_D \cos(\theta)\tau}]e^{j\omega_D \cos(\theta_0)\tau}\}] \quad (14)$$

which is a generalization of the result derived in Reference [8] where $r_x(\tau)$ was assumed to be real. Assuming Equation (5) and using Equation (6), the general expression in Equation (14) becomes:

$$c_{|h|^2}(\tau) = \frac{1}{(K+1)^2} \times \left[\left| J_0\left(\sqrt{-\kappa^2 + \omega_D^2\tau^2 - 2j\kappa\cos(\alpha)\omega_D\tau}\right)/I_0(\kappa) \right|^2 + 2K\mathcal{R}\left\{ J_0\left(\sqrt{-\kappa^2 + \omega_D^2\tau^2 - 2j\kappa\cos(\alpha)\omega_D\tau}\right) \times e^{j\omega_D \cos(\theta_0)\tau}/I_0(\kappa) \right\} \right]$$

Notice that when $K = \kappa = 0$, Equation (14) reduces to $c_{|h|^2}(\tau) = J_0^2(\omega_D\tau)$.

The mean and covariance of $H(t)$ are useful when the dB value of the power $P(t)$ is used for velocity or local mean estimation. We provide expressions for both, assuming $K = 0$ (Rayleigh fading). The mean of $H(t)$ can be shown to be [14, 15],

$$\overline{H} := E[H(t)] = -\frac{10}{\ln(10)}\gamma \quad (15)$$

where $\gamma = 0.577216\ldots$ is Euler's constant. The covariance denoted by $c_H(\tau)$ has been derived in References [16–18], with Reference [16] containing the simplest form as:

$$c_H(\tau) = \left[10/\ln(10)\right]^2 \sum_{k=1}^{\infty} \frac{q^k(\tau)}{k^2} \quad (16)$$

where $q(\tau) := |E[\exp(j\omega_D\tau\cos\theta)]|^2$ which, with the $K = 0$ assumption becomes $q(\tau) = |J_0(\sqrt{-\kappa^2 + \omega_D^2\tau^2 - 2j\kappa\cos(\alpha)\omega_D\tau})/I_0(\kappa)|^2$ if the AOA is given by Equation (5). The infinite series in Equation (16) can be approximated well with a polynomial in $q(\tau)$ for $q(\tau) \in (-1, 1)$. In Reference [14] this fact is used to approximate Equation (16) in terms of $q(\tau)$ and $q^2(\tau)$ with high accuracy using numerical techniques. A simpler approximation that is valid for small τ has been utilized in References [17] and [18] and is given by $c_H(\tau) \approx \left[10/\ln(10)\right]^2 (\pi^2/6)q(\tau)$.

2.2. Shadow Fading Statistics

The dB value of the shadow fading, $S(t)$, is commonly modeled as a Gaussian process with mean μ_S and variance σ_S^2. The mean is given by the path loss which decreases monotonically with the MS–BS distance. However, for the purposes of local mean and velocity estimation, μ_S can be assumed to be constant during the time that the received signal is processed [2, 14].

A first order autoregressive model for the shadowing process suggested in Reference [19] is based on the measured autocovariance function of $S(t)$ in urban and suburban environments (for another set of empirical results see Reference [20]):

$$c_S(\tau) = \sigma_S^2 \exp(-v|\tau|/X_c) \quad (17)$$

where X_c is the so-called effective correlation distance. The pair (σ_S, X_c) can vary from (4.3 dB, 10 m) in urban environments to (7.5 dB, 500 m) in suburban areas [19]. The shadow variance plays an important role in the selection of the hysteresis in handoff algorithms and, as we will see, the correlation distance X_c affects the optimum window size selection for local power estimation. A modified expression for $c_S(\tau)$ is proposed in Reference [21] and has a well-defined ZCR, unlike Equation (17).

To sum up, the multipath component $h(t)$ in Equation (3) is a complex Gaussian process with a correlation function given in Equation (6) and spectrum in Equation (7), which reduces to Clarke's model when $\kappa = 0$ corresponding to a uniform AOA. The level crossing rate of the Ricean process $|h(t)|$ is given in Equation (12), the zero crossing rate of $\mathcal{R}\{h(t)\}$ is given in Equation (13), and the covariance function of $|h(t)|^2$ is expressed in Equation (14). The dB value of the multipath process, $H(t)$, has a mean given by Equation (15) and covariance function by Equation (16). The dB value of the shadow process, $S(t)$, is Gaussian with mean determined

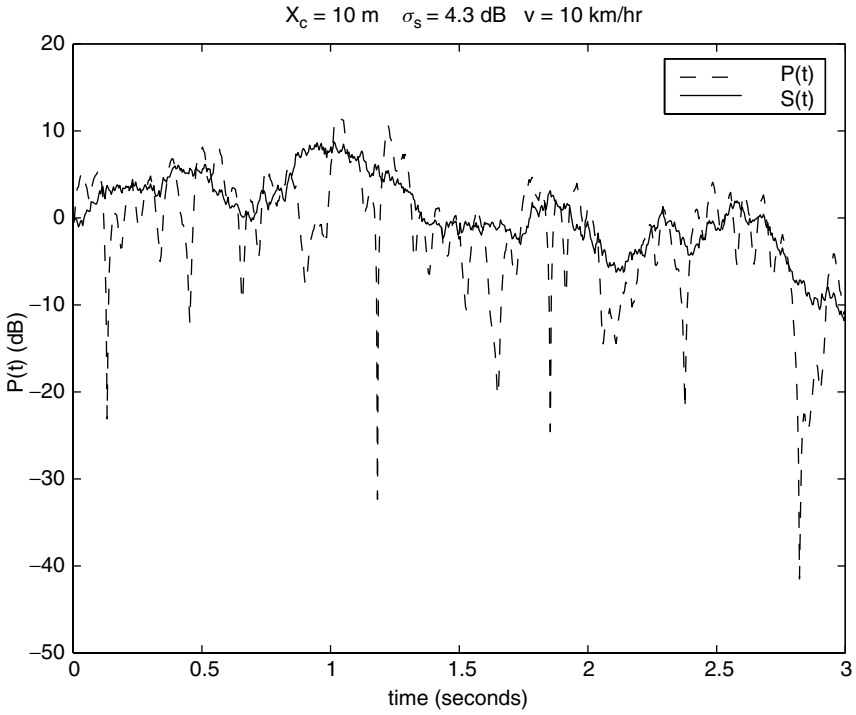

Fig. 3. Simulated received power in an urban environment.

by the pathloss and covariance function given by Equation (17). These quantities play an important role in the design and performance of local power and velocity estimators.

In Figure 3 we illustrate the simulated dB value of the received power around μ_S in an urban environment with $X_c = 10$ m, $\sigma_S = 4.3$ dB, and $v = 10$ km hr^{-1}. The goal of local power estimation is to filter out the fast fading from the received power $P(t)$ to obtain an accurate estimate of the shadow variations $S(t)$. We give an overview of the local power estimation in the next section, after a brief overview of the more general topic of channel quality estimation.

3. Channel Quality Estimation

It is well known that the channel quality, which ultimately determines whether the communication system under consideration can meet the specified quality of service requirements, depends on the value of the local mean $S(t)$ (or $s(t)$), the Ricean K factor, and the parameters X_c and σ_S which depend on the propagation environment. Measures of channel quality which incorporate noise and interference are most indicative of system performance, but they require considerably more signal processing than the simple local power estimation schemes. We briefly mention some of the literature on signal to interference plus noise ratio (SINR) estimation without going into technical details owing to lack of space, before we start a detailed discussion of local power estimation.

Unlike the local power estimation schemes, the SINR estimation techniques exploit the digital modulation that is employed. In Reference [22] (see also Reference [2]) the authors use a training sequence, or decisions made by the detector to estimate the signal and interference plus noise power which are used to calculate the SINR. The information that the eigenvalues of the output covariance matrix convey about the signal and noise powers is exploited in Reference [23] for SINR estimation. A projection based approach that generalizes Reference [22] is proposed in Reference [24] and is shown to have approximately the same performance as Reference [23] despite its lower computational complexity. The error metric in a Viterbi decoder is utilized in Reference [25] for SINR estimation for both differential and coherent detection. Recently in Reference [26], four different signal to noise ratio (SNR) estimators designed for QPSK modulation are compared.

In the sequel we focus on local power estimation methods for assessing channel quality, since they are

more prevalent in practice because of their simplicity. Then we briefly outline approaches for the estimation of the Ricean K factor, X_c and σ_S which are important in evaluating the severity of fading and useful in appropriate selection of hysteresis for handoff algorithms [27, 28].

3.1. Local Power Estimation

We begin this subsection by providing some basic results on local power estimation [2, 29–31] and the effects of $\boldsymbol{\psi}$ on the estimation error. We then discuss the approach in Reference [14] and explain how it differs from the existing techniques. We conclude this subsection by outlining two recent papers about local power estimation that offer novel ideas but demand high computational complexity [15, 33].

In estimating the local power, one could work with Equations (1) or (2) depending on whether the power amplifier is linear or logarithmic. In either case, the problem is to average the instantaneous received power so as to remove the fast multipath fading, but follow the variations of the slower shadow fading. This is possible by the appropriate choice of the averaging filter bandwidth or, equivalently, the suitable averaging window size. We first consider the multiplicative model in Equation (1), originally proposed in Reference [30] and subsequently used in References [2, 29, 31]. The goal in the aforementioned references is, in part, to find the appropriate averaging distance $2L$ in terms of the wavelength λ. The necessary averaging *duration*, then, would be found through knowledge of the velocity v. So, in what follows, we temporarily assume that $v = \lambda$ m sec^{-1} ($\omega_D = 2\pi$ rad sec^{-1}) in order to be able to express all quantities as a function of distance, and find the optimum window length in terms of number of wavelengths.

The estimator for $s(d)$ can be expressed as[¶]:

$$\hat{s}(d) := \frac{1}{2L}\int_{d-L}^{d+L} p(l)dl = \frac{s}{2L}\int_{d-L}^{d+L} |h(l)|^2 dl \tag{18}$$

where it is assumed that the shadow fading is approximately constant and equal to s during the averaging interval, i.e. $s(d) \approx s$, for $d \in [d-L, d+L]$. Note that $\hat{s}(d)$ is an unbiased estimator. The accuracy of the estimator $\hat{s}(d)$ in Equation (18) is measured by its variance which can be shown to be [30]:

$$\sigma_{\hat{s}}^2 = \frac{s^2}{L}\int_0^{2L}\left(1 - \frac{l}{2L}\right) c_{|h|^2}(l)dl \tag{19}$$

where $c_{|h|^2}(l)$ is given by Equation (14). Recall that $c_{|h|^2}(l)$ depends on $\boldsymbol{\psi} = [K, \theta_0, \kappa, \alpha]$. However, for all the values of $\boldsymbol{\psi}$ that we considered, Equation (19) monotonically decreases with L. We illustrate this in Figure 4, where we plot the 1σ spread $:= 10\log((s+\sigma_{\hat{s}})/(s-\sigma_{\hat{s}}))$, versus the averaging window size in wavelengths. The 1σ spread, defined in Reference [30], is a monotone increasing function of $\sigma_{\hat{s}}$, and is zero when $\sigma_{\hat{s}} = 0$, therefore it is an alternative measure of the estimation error. Assuming that the window size $2L$ is big enough to make $\hat{s}$ a Gaussian random variable, the 1σ spread has the interpretation that $Prob(|\hat{s}_{\mathrm{dB}} - s_{\mathrm{dB}}| < 1\sigma\text{spread}) > 0.68$, where $\hat{s}_{\mathrm{dB}}$ and s_{dB} are the dB values of $\hat{s}$ and s respectively. The appropriate window length is the minimum value of $2L$ that yields a satisfactory $\sigma_{\hat{s}}^2$ over a realistic range of $\boldsymbol{\psi}$. We would like to keep L as small as possible, since the error due to the shadow variations increases with L and is not accounted for by the error measure in Equation (19). From Figure 4, $2L = 20\lambda$ seems to be the right window size since any further increase in L does not bring significant improvement on the 1σ spread.

In Reference [29], the authors studied the effects of K and θ_0 on the 1σ spread in detail. They observed that increasing K decreases the 1 σ spread as shown in Figure 4 (left). This is intuitive since increasing K causes the fading to have less severe fluctuations which makes estimates of its mean value less prone to error. The effect of directional scattering on local power estimates, however, is not considered in Reference [29]. In Figure 4 (right) we show that a more directional reception (larger κ) increases the error in the local power estimate. Although not shown, we observed that for nonzero values of α and K, the increase in the 1σ spread with κ, although present, was less pronounced.

In Reference [30], Lee and Yeh considered the effect of finite M (number of multipath components) in Equation (3), on $\sigma_{\hat{s}}^2$ and showed that increasing M increases the error. As for the effect of the LOS direction, it is shown in Reference [29] that $\theta_0 = \pi/2$ (a time invariant LOS component $y(t)$ in Equation (3)), yields the smallest 1σ spread, which we illustrate in Figure 5.

[¶] Reference [30] also considers signal strength estimation from the received envelope $\sqrt{p(t)}$ and argues that the results are similar to that obtained from $p(t)$. Hence, we do not consider local mean estimation using $\sqrt{p(t)}$ herein.

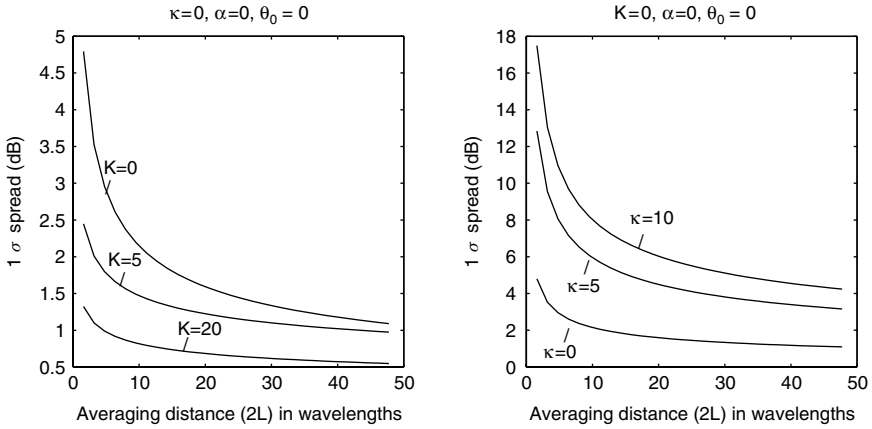

Fig. 4. 1σ spread versus averaging distance $2L$ in wavelengths for various K and κ.

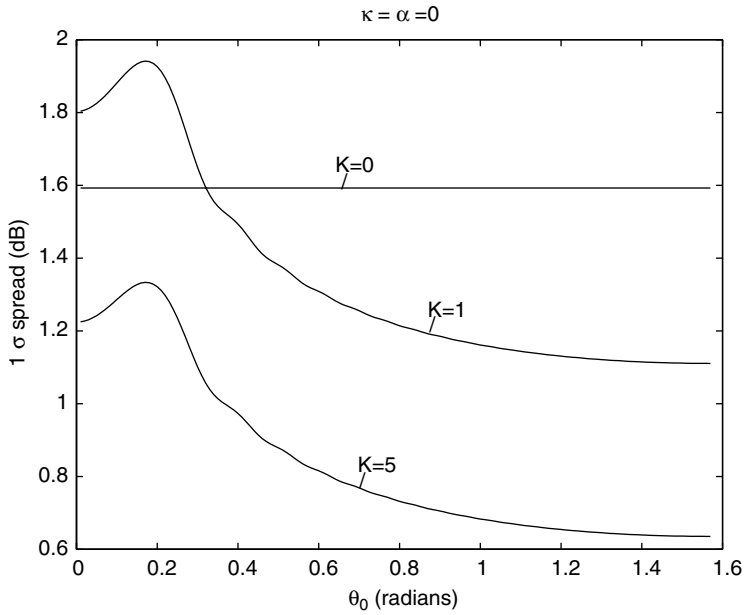

Fig. 5. Effect of θ_0 on the 1 σ spread.

Instead of analog averaging, implementable with an integrate-and-dump circuit, often samples of the received power $p(nT_s)$ are employed in estimating the shadow fading, where T_s denotes the sampling duration[||]. A reasonable unbiased estimator then would be:

$$\hat{s} = \frac{1}{N}\sum_{n=0}^{N-1} p(nT_s) \tag{20}$$

where again the shadowing is assumed to be constant over NT_s seconds. The variance of $\hat{s}$ can be shown to be [29, 30]:

$$\sigma_{\hat{s}}^2 = s^2\left[\frac{c_{|h|^2}(0)}{N} + 2\sum_{k=1}^{N-1}\left(\frac{N-k}{N^2}\right)c_{|h|^2}(kT_s)\right] \tag{21}$$

What is an appropriate value for T_s in terms of λ? If we fix the number of samples N, then choosing T_s large results in approximately uncorrelated samples, yielding a reduction in $\sigma_{\hat{s}}^2$. This is illustrated in Figure 6 (left) where it is observed that while increasing T_s decreases the error, a $T_s > \lambda$ does not

[||] We continue to assume that $v = \lambda$ m sec^{-1} so that T_s is also the spatial distance in wavelengths between two adjacent samples.

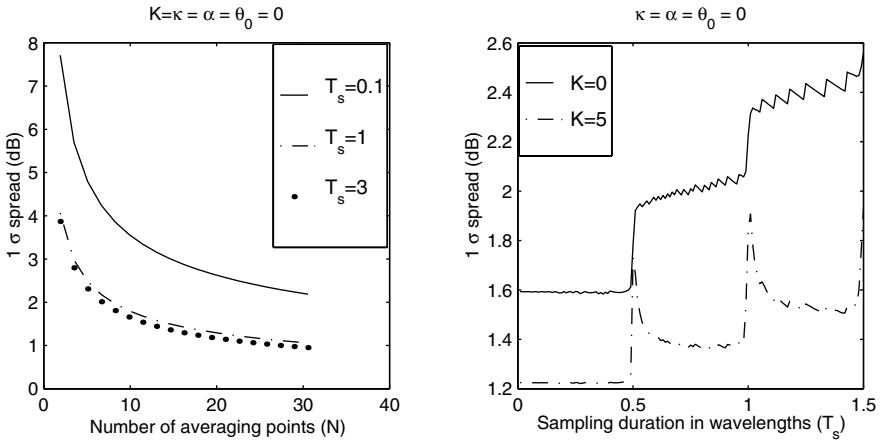

Fig. 6. Effect of sampling on 1 σ spread.

bring significant reduction in the 1σ spread. On the other hand, we would like T_s to be as small as possible for a fixed N so as to have a short window of averaging over which $s(t)$ has not changed significantly. This prompts us to fix the averaging window size to a nominal value (20 λ in Figure 6 (right)) and ask what value of T_s would be small enough to get sufficient number of samples N so that the sum in Equation (20) approximates the integral in Equation (18). We show in Figure 6 (right) that $T_s < 0.5\lambda$ suffices for both $K = 0$ and $K = 5$, as also shown in Reference [29].

The approaches described so far have assumed that the shadow process is constant over the duration of the averaging window, and have utilized $p(t)$ in estimating $s(t)$. In contrast to existing approaches, Reference [14] proposes estimators for both $S(t)$ and $s(t)$ depending on whether the signal is measured through a linear or logarithmic amplifier. This is important since most handoff algorithms rely on estimates of the dB value of the shadow process. We illustrate the approach in Reference [14] in Figure 7, where the received signal passes through a square law envelope detector, is amplified with a linear or logarithmic amplifier, and filtered through an averaging filter. The impulse response of the averaging filter is restricted to be an integrate-and-dump (ID), or a first order RC filter because of practical constraints, and

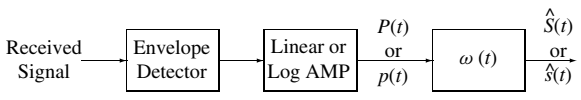

Fig. 7. Block diagram depicting the approach in Reference [14].

is given by:

$$w_{\mathrm{ID}}(t) = k\frac{1}{T_{\mathrm{ID}}}\ \mathrm{Rect}\ \left(\frac{t}{T_{\mathrm{ID}}} - \frac{1}{2}\right)$$
$$w_{\mathrm{RC}}(t) = k\frac{1}{T_{\mathrm{RC}}}\exp\left(\frac{-t}{T_{\mathrm{RC}}}\right) \qquad (22)$$

where $\mathrm{Rect}(t) = 1$ for $0 \le t \le 1$ and 0 else, k is the DC value of the filters' frequency responses, and T_{ID}, T_{RC} control the averaging duration. It is argued in Reference [14] that the estimation errors $\hat{S}(t) - S(t)$ for the so-called log-power method and $10\ \log(\hat{s}(t)/s(t))$ for the linear-power method are both approximately Gaussian, and that the estimation bias could be removed by the proper choice of k in Equation (22). The appropriate averaging duration, then, is selected by optimizing the time constants T_{RC} and T_{ID} so as to minimize the estimation error variance for both the linear-power and log-power methods. It is shown that the shape of the filter (ID or RC), or whether $p(t)$ or $P(t)$ is averaged, did not influence the error significantly. However, the proper choice of the filter time constants is shown to be crucial.

A significant departure from the conventional approach for local power estimation that Reference [14] exhibits is incorporation of the shadow variations in the error criterion by allowing for a variable local mean over the averaging window duration. Hence, the optimal window size not only depends on the vehicle velocity, but also on the shadow fading characteristics σ_S and X_c. In Figure 8, for a carrier frequency of 1 GHz (corresponding to $\lambda = 0.3$ m), we illustrate the effect of the pair (σ_S, X_c) on the root mean squared (RMS) dB error where an integrate-and-dump filter with $T_{\mathrm{ID}} = 0.085$ s is employed. For $(\sigma_S, X_c) = (4.3\ \mathrm{dB}, 25\lambda)$, corresponding to measured

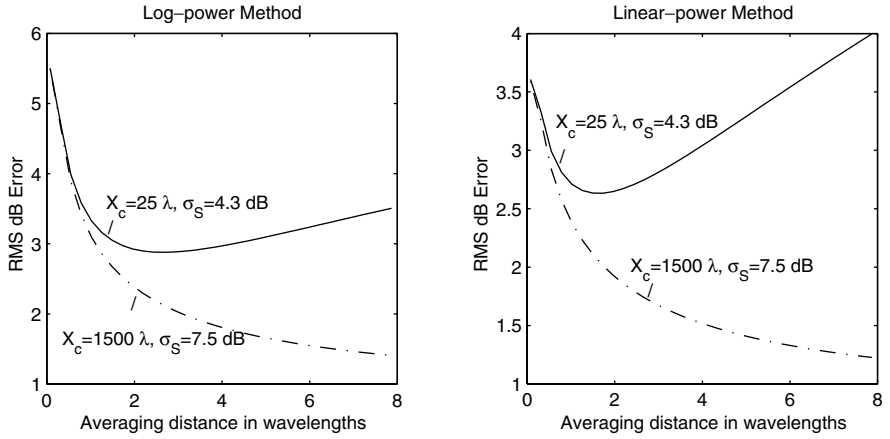

Fig. 8. Effect of shadow correlation on performance of local power estimators in Reference [14].

values for an urban area [19], the shadow variation is relatively fast and results in increasing error if the averaging distance is more than ($\approx 2\lambda$). This means that in an urban environment where the averaging distance is beyond $\approx 2\lambda$, the performance of the local mean estimator deteriorates. This could not be predicted with the previous approaches where the error always reduced with averaging distance (c.f. Figure 4). On the other hand, in suburban environments where the shadow fading is much more correlated with a correlation distance of $X_c \approx 1500\lambda$ [19], increasing averaging distance still improves the local power estimator performance for both the linear-power and log-power methods. Hence, the appropriate averaging distance depends on the effective shadow correlation distance X_c and the shadow variance σ_S^2, which are defined by the degree of urbanization. Even though implied by the findings in Reference [14], this fact has not been articulated in the literature. In analyzing user membership, the authors in Reference [32] have observed a similar effect, where a certain window size is found to be optimum in terms of minimizing the probability of wrong selection.

Reference [14] also discusses the effects of the unknown parameters v, X_c, and σ_S and suggests how to make the local power estimators robust to the variability of these parameters. Also, the benefits of broadband reception and/or multiple antennas are briefly delineated in Reference [14], where processing independent multipath components that are superimposed on the same shadow component is shown to reduce the estimation error. The practical impact of Reference [14] is in showing that a fixed filter design can keep the estimation error within 3 dB over a realistic range of mobile velocities and shadow fading characteristics.

We conclude this subsection by outlining two recent approaches to local power estimation that are computationally more demanding than linear filtering (averaging) of the received power, on which the aforementioned methods have relied. Consider first the simulated received power in Figure 3. A possible approach to tracking the shadow fading is to average the received power at samples of the composite multipath-shadow fading that are near the shadow fading. In Reference [33] the authors proposed using t_n^{mid}, the midpoints of the local minima as sampling locations to calculate the local power $s(t) \approx s$, assumed constant over the averaging window. Hence the proposed estimator in Reference [33] is $\hat{s}_{\text{mid}} := CN^{-1} \sum_{n=0}^{N-1} p(t_n^{\text{mid}})$, where the constant C is determined empirically. The locations of the local minima were estimated using the modulus maxima of $P(t)$'s continuous wavelet transform (CWT). The authors assumed that $K = \kappa = 0$. The results suggest that this wavelet-based scheme outperforms existing techniques when the velocity changes rapidly. Even though promising in high variability environments, this method seems to be highly model-dependent (the appropriate value of C depends on $\boldsymbol{\psi}$ which is not known *a priori*), and is more computationally demanding than existing approaches.

Assuming a constant $S(t) \approx S$ during the averaging window and a large enough T_s to assure *independent samples* $P(nT_s)$, a minimum variance unbiased estimator for S was derived in Reference [15] to be:

$$\hat{S}_{\text{MVU}} := 10 \left[\log \left(\sum_{n=0}^{N-1} |p(nT_s)|^2 - \frac{\sum_{n=1}^{N-1} \frac{1}{n}}{\ln(10)} \right) \right] - \overline{H} \tag{23}$$

where $\overline{H}$ is given in Equation (15) and can be precomputed. It is argued in Reference [15] that the sample mean estimator $\hat{S}_{\mathrm{SM}} := N^{-1}\sum_{n=0}^{N-1} P(nT_s) - \overline{H}$ is also unbiased and consistent like $\hat{S}_{\mathrm{MVU}}$, but the variance of $\hat{S}_{\mathrm{MVU}}$ is approximately 1.6 times smaller than that of $\hat{S}_{\mathrm{SM}}$ for $N \geq 15$. This gain in performance is shown to translate into a reduction of N by a factor of approximately 2/3 for a fixed 1 σ spread. While the Cramér-Rao bound for this problem cannot be achieved by any unbiased estimator, Equation (23) achieves this bound asymptotically, i.e. $\hat{S}_{\mathrm{MVU}}$ is asymptotically efficient. The effect of a LOS component is evaluated in Reference [15] by simulation and for $K > 0.5$, the mean-squared error is shown to increase owing to an increase in the bias of $\hat{S}_{\mathrm{MVU}}$. Hence, the estimator is found appropriate for environments where an LOS component is weak or not present. Although Reference [15] is a contribution of theoretical importance, the conflicting assumptions of independent samples of $P(t)$ and constant $S(t)$, together with increased computational complexity are seen to be its shortcomings.

In Reference [34], efficient measurement techniques for local power estimation in indoor environments are proposed. It is found experimentally that using a window of size 10 λ provides sufficient averaging without significantly distorting the shadow fading.

3.2. Estimating the Ricean Factor, Shadow Variance, and Shadow Correlation Distance

As we mentioned before, $|h(t)|$ is a Ricean process with parameter K. It is well known that the value of K is a measure of the severity of fading with $K = 0$ being the most severe Rayleigh fading, and $K = \infty$ representing no fading. Hence, the knowledge of the K-factor is a good indicator of the channel quality and is important in link budget calculations [35]. The presence of the LOS component also influences velocity estimators and local power estimators which make the estimation of K an area of interest. Greenwood and Hanzo in Reference [35] have proposed techniques for estimating K that fit the empirical distribution of the envelope $|h(t)|$ to the Rice distribution, but these techniques are not well suited for online estimation. More recently, Greenstein *et al.* introduced a moment-based method for estimating K under the assumption that the LOS angle of arrival $|\theta_0| = \pi/2$ (i.e. $E[h(t)]$ is a time-invariant constant) [36]. Here, we briefly describe the approach for estimating K from $p(t)$ that was originally proposed in Reference [36], and show that it is also valid when $|\theta_0| \neq \pi/2$ (i.e. when the LOS component $y(t)$ depends on time).

We make the usual assumption that the shadow fading is constant during the course of the estimation, i.e. $p(t) \approx s|h(t)|^2$. This means that the covariance of $p(t)$ is $c_p(\tau) = s^2 c_{|h|^2}(\tau)$. Setting $\tau = 0$ and using Equation (14) we obtain $c_p(0) = s^2(1 + 2K)/(K + 1)^2$. By solving the resulting quadratic equation for K in terms of s^2 and $c_p(0)$ we find:

$$K = \frac{s^2 - c_p(0) + s\sqrt{s^2 - c_p(0)}}{c_p(0)} \tag{24}$$

which is the result in Reference [36]. Since s^2 and $c_p(0)$ can be estimated from $p(t)$, Equation (24) provides us with an estimate of K.

As pointed out before, the shadow parameters X_c and σ_S depend on the propagation environment and have a significant impact on the proper averaging window size for local power estimation, and selection of handoff algorithm parameters. Since X_c and σ_S are defined through the covariance function of $S(t)$, estimating these parameters entails estimating $c_S(\tau)$ in Equation (17). Having only access to $P(t)$, one approach is to estimate $S(t)$, using the previously described techniques, and then use $\hat{S}(t)$ to estimate the shadow parameters. But it should be kept in mind that unless the averaging filter is all-pass, the spectral properties of $S(t)$ are different from that of $\hat{S}(t)$. In Reference [28] the authors used estimates of $S(t)$ to estimate the shadow parameters, taking the effects of the averaging filter into account. More recently, the authors in Reference [37] have assumed access to $S(t)$ in designing shadow parameter estimators that exhibit good bias properties, but neglected the effect of the averaging filter that would need to be used to obtain $S(t)$. Here, we illustrate that X_c and σ_S can be estimated directly from $P(t)$ using $c_H(\tau)$ in Equation (16) and $\overline{H}$ in Equation (15). Consider the autocorrelation function of the sampled power $P(nT_s)$:

$$r_P(mT_s) := E\left[P(nT_s)P(nT_s + mT_s)\right] = c_H(mT_s) + (\overline{H}^2 + \mu_S)^2 + \sigma_S^2 \exp(-vmT_s/X_c) \tag{25}$$

where we used Equation (2), the independence of $H(t)$ and $S(t)$, and Equation (17). Assuming that the vehicle velocity v is already estimated, the first two terms on the right-hand side of Equation (25) are precomputable for each lag m and can be subtracted from $r_P(mT_s)$. The shadow mean μ_S can be estimated using the sample mean of $P(nT_s)$ and knowledge of $\overline{H}$ since $E[P(t)] = \overline{H} + \mu_S$. This means that, having

knowledge of v (see Section 4 for estimators of v), an estimate $\hat{r}_P(mT_s)$ can be used to obtain an estimate of $c_S(mT_s)$ in Equation (17) for every lag m. Then one can proceed from $\hat{c}_S(\tau)$ in a number of ways to obtain X_c and σ_S^2. A naive approach is to set $\tau = 0$ and estimate σ_S^2, and then use this estimator and $\tau > 0$ to estimate X_c, but it has been shown in Reference [37] that an estimate of σ_S^2 obtained with such a procedure has a large bias. A more sophisticated method could use Equation (25) for $m = 0, \ldots, T$, to obtain μ_S, σ_S and X_c utilizing regression techniques. Exploration of other possible estimators exploiting Equation (25) with good bias and variance properties is still a future research topic.

All through our discussion of local power estimation and estimation of shadow parameters, we saw that an accurate knowledge of the velocity v, or its proportional surrogate ω_D is essential. We give a detailed discussion of velocity estimation techniques in the next section.

4. Velocity Estimation

Doppler-based velocity estimation has a rich history and a diverse range of applications (see Reference [38] and references cited therein). In HF communication applications, Bello [6] was one of the first to propose techniques for the estimation of a variance-like RMS measure of the Doppler spectrum $S_h(\omega)$ that used $h(t)$ or $|h(t)|$. A study of the accuracy of these estimators can be found in Reference [39].

More recently, in mobile communications, estimation of the mobile velocity, or equivalently the maximum Doppler spread has received considerable attention. In what follows we briefly summarize the literature in this area, before going into technical details. As we saw in the previous section, knowledge of v is necessary for the appropriate choice of averaging window length, which was originally brought to light in the pioneering works of Holtzman–Sampath [18], and Austin–Stüber [29], where they proposed velocity estimators that rely on the covariance or the LCR of the multipath signal ($H(t)$ or $h(t)$). Lin and Proakis also proposed a Doppler estimator for adaptive channel tracking applications that used the I/Q components of the estimated channel in a TDMA system [40]. Subsequently, eigen-based Doppler estimators for continuous-phase modulation were proposed in Reference [41]. Switching rate of diversity branches is exploited in Reference [42] for Doppler estimation, and extensions of this idea are reported in Reference [43]. Online change detection techniques are combined with LCR of the envelope in Reference [44]. Reference [45] uses the so-called 'higher-order crossings' (HOC) (zero-crossings of the derivatives) of the envelope and is the first to use a parametric AOA distribution for assessing velocity estimator performance in nonisotropic scattering propagation environments (i.e. nonuniform AOA distributions). An approximate average maximum likelihood estimator with an FFT-based digital implementation can be found in Reference [46]. Fluctuations of the channel power in closed-loop power control and constant power scenarios are considered in Reference [47] for velocity estimation. A thorough analysis of the model error incurred by a class of covariance-based estimators due to $\boldsymbol{\psi} \neq \mathbf{0}$ can be found in Reference [48]. A wavelet-based scheme that estimates the velocity by locating the minima of the received envelope is reported in Reference [49]. The curvature of the estimated autocorrelation function at zero is used in References [13] and [50] for estimation of ω_D, and promises to be useful especially for adaptive modulation, coding, and interleaving applications.

In this section we discuss some of the schemes mentioned earlier in detail. We categorize Doppler-based velocity estimators as LCR-based estimators and those that rely on the covariances of $H(t)$ or $h(t)$. Figure 9 illustrates the taxonomy of the velocity estimators that we discuss further in this section. We should note that throughout the literature, the estimated velocity and the shadow variation is assumed to be constant during the estimation process, even though robustness of estimators to the variability of the velocity and the shadow fading has been considered. Hence, in this survey we will assume that the velocity and the shadowing are approximately constant during the estimation process. It should also be noted that since the estimation of the parameters $\boldsymbol{\psi} = [K, \theta_0, \kappa, \alpha]$ is not always feasible, all the velocity estimators in Figure 9 are designed assuming $\boldsymbol{\psi} = \mathbf{0}$ (uniform AOA distribution with no LOS

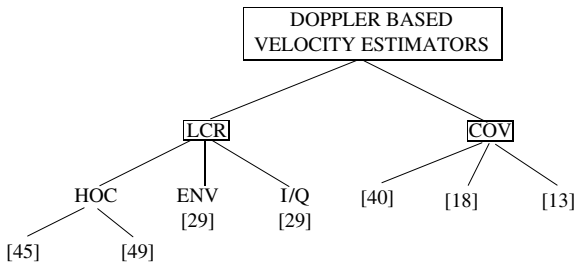

Fig. 9. Taxonomy of velocity estimators discussed in this paper.

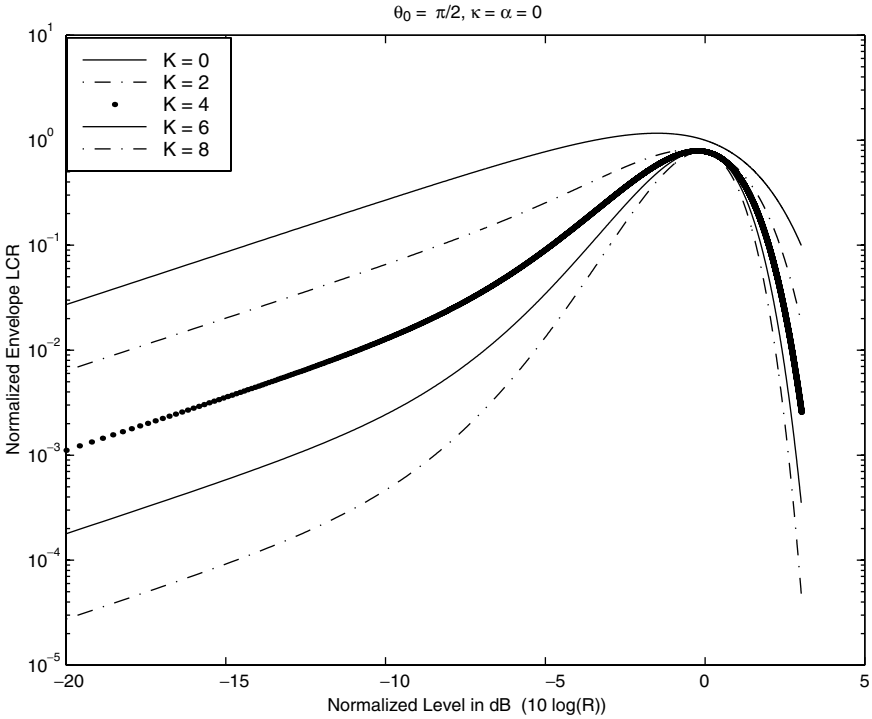

Fig. 10. Choice of level R for LCR estimators robust to variations in K.

component) and absence of noise; we will attempt, whenever tractable, to express the effects of the modeling error incurred by $\boldsymbol{\psi} \neq \mathbf{0}$ and the error caused by noise on these estimators. In the absence of noise, $\boldsymbol{\psi} \neq \mathbf{0}$ causes the estimator to be scaled. This scale factor $A(\boldsymbol{\psi})$ will be derived for each estimator. The estimation error due to finite number of samples is also characterized at the end of this section. We begin by discussing the LCR-based estimators in the next subsection, and then move on to covariance-based estimators.

4.1. LCR-based Velocity Estimators

It is well known that the LCR of the envelope, or the ZCR of the I/Q components are proportional to ω_D and offer a low complexity approach to velocity estimation [2]. We begin by discussing the envelope LCR estimator.

As mentioned in Section 2.1, we can use Equation (12) to obtain $\mathrm{LCR}(R, \mathbf{0}) = (\beta/2\pi)^{1/2}$ $(R/r_x(0)) \times \exp[-R^2/(2r_x(0))] = (\omega_D/\sqrt{2\pi})R$ $\exp(-R^2)$, which is a multiple of ω_D that depends on the known level R. In Reference [29], the authors investigated what value of R would make the envelope LCR estimator robust to variations of K. They found that if the level is chosen as the RMS value of the received power, which without loss of generality we assume to be $[E|h(t)|^2]^{1/2} = 1$, then K has little influence on the envelope LCR. This is illustrated in Figure 10, where we see that the curves corresponding to different K's cluster together around $R = 1$. In general, a $\boldsymbol{\psi} \neq \mathbf{0}$ scales the estimator where the scale factor is *independent* of ω_D, given by $A_{\mathrm{LCR}}(R, \boldsymbol{\psi}) := \mathrm{LCR}(R, \boldsymbol{\psi})/\mathrm{LCR}(R, \mathbf{0})$, which can be calculated using Equation (12) and numerical integration. Using this approach, we illustrate the joint effect of K and κ on the scale factor $A_{\mathrm{LCR}}(1, \boldsymbol{\psi})$ for $\theta_0 = \alpha = 0$ and $\theta_0 = \alpha = \pi/2$ in Figure 11. Especially for $\theta_0 = \alpha = 0$, the envelope LCR estimator is seen to be robust to variations in K and κ. The effect of additive Gaussian noise** $n(t)$, which is assumed to be independent of $h(t)$, can also be characterized through β, ξ, and ρ by replacing $r_x^{(k)}(0)$ with $r_x^{(k)}(0) + r_n^{(k)}(0)$, $k = 0, 1, 2$ (c.f. Equation (12)) [29, 45]. Note the interesting fact that $\mathrm{LCR}(R, \boldsymbol{\psi})/\mathrm{LCR}(R, \mathbf{0})$ does depend on ω_D whenever additive noise is present.

We follow a similar approach for the ZCR of the I/Q components given by Equation (13) which reduces to $\mathrm{ZCR}(\mathbf{0}) = \pi^{-1}[-r_x''(0)/r_x(0)]^{1/2} = \omega_D/(\sqrt{2}\pi)$. Like the envelope LCR, the I/Q

** Note that the additive noise corrupts $h(t)$ and not $|h(t)|$.

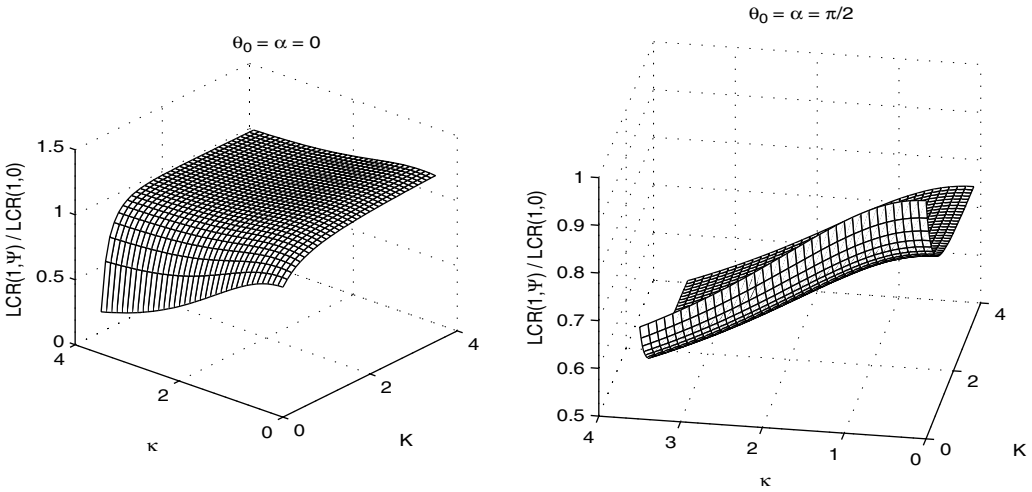

Fig. 11. Sensitivity of the envelope LCR to K and κ.

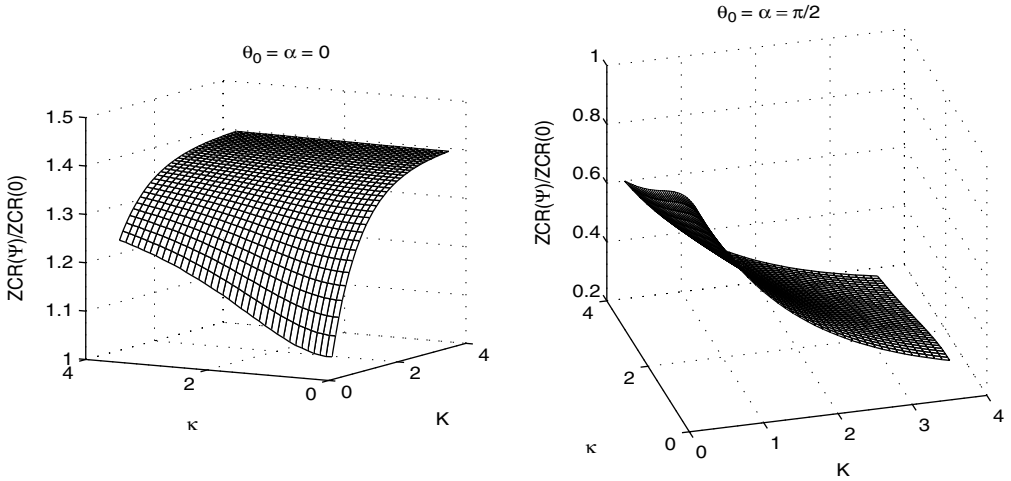

Fig. 12. Sensitivity of ZCR (I/Q) estimators to K and κ.

ZCR is proportional to ω_D and therefore can be used as a velocity estimator. The ZCR estimator designed for $\boldsymbol{\psi} = \mathbf{0}$ scales by a factor $A_{\mathrm{ZCR}}(\boldsymbol{\psi}) := \mathrm{ZCR}(\boldsymbol{\psi})/\mathrm{ZCR}(\mathbf{0})$, which is independent of ω_D in the absence of noise. In Figure 12, we illustrate $A_{\mathrm{ZCR}}(\boldsymbol{\psi})$ as a function of K and κ for $\theta_0 = \alpha = 0$ and $\theta_0 = \alpha = \pi/2$. We notice that the scale function is not as robust to variations in K and κ as the envelope LCR estimator. The effect of additive noise can be calculated the same way as outlined for the envelope LCR method. Again we see that the presence of noise renders the scale factor dependent on ω_D.

The rate of maxima (ROM) of the envelope, which is the ZCR of the envelope derivative, is utilized in Reference [45] for velocity estimation. The authors use an accurate approximation of the ROM in designing an estimator for ω_D. This approach circumvents the necessity for a reliable local power estimator, which is required for both the envelope LCR and ZCR methods previously mentioned. Also in Reference [45], the effect of nonisotropic scattering on velocity estimators is formulated analytically by using the von Mises distribution in Equation (5). It is shown that the ROM estimator is more robust to nonisotropic scattering and noise than the I/Q ZCR estimator. The effect of shadowing is also considered in Reference [45], while the impact of a LOS component is addressed in Reference [51].

Similar to the method used in Reference [45], the authors in Reference [49] use the rate of envelope minima for velocity estimation. The locations of the local minima are estimated using the modulus maxima

of $P(t)$'s CWT (much like Reference [33]), with the assumption that the logarithmic quantity $P(t)$ has discontinuous derivatives at its local minima. This assumption is necessary since the CWT is used to detect the singularities of $P(t)$ which are characterized by its discontinuous derivatives. By relating the zero crossings of the envelope derivative to ω_D, the authors propose a rate of minima estimator similar to Reference [45], wherein they also provide a wavelet-based approach for obtaining the locations of the minima. The authors prove that the rate of minima is independent of the received power, which shows that the estimator does not suffer from inaccurate local power estimation. However, neither the presence of noise nor the effect of $\boldsymbol{\psi} \neq \mathbf{0}$ is considered in Reference [49].

4.2. Covariance/Correlation-based Velocity Estimators

Lin and Proakis were among the first to tackle the estimation of ω_D using correlations of channel estimates [40]. Assuming $\boldsymbol{\psi} = \mathbf{0}$, they proposed the following nonlinear correlation matching approach to Doppler estimation:

$$\hat{\omega}_D^{\mathrm{LP}} = \underset{\omega_D}{\operatorname{argmin}} \sum_{k=0}^{N-1} \left[J_0(\omega_D k T_s) - \hat{r}_h(kT_s) \right]^2 \qquad (26)$$

where $\hat{r}_h(kT_s)$ is the normalized sample correlation estimator so that $\hat{r}_h(0) = 1$. To make the nonlinear least squares problem in Equation (26) tractable, the authors, upon taking the derivative with respect to ω_D to perform the optimization in Equation (26), approximate $J_0(x)$ with the first few terms (6 to 8 in Reference [40]) of its power series expansion which turns the problem into one of polynomial root finding. The coefficients of the polynomial depend on $\hat{r}_h(kT_s)$, and the roots are found using Newton's method. The final estimate is obtained as an average over 10 to 20 TDMA frames. The effect of the SNR and the number of frames is illustrated by simulation, but $\boldsymbol{\psi} \neq \mathbf{0}$ is not considered.

In Reference [18], Holtzman and Sampath proposed a covariance-based Doppler estimator using the formula:

$$\hat{\omega}_D^{HS} := \frac{C}{T_s} \sqrt{\frac{V(T_s)}{\hat{c}_z(0)}} \qquad (27)$$

where:

$$V(T_s) := \frac{1}{N} \sum_{n=0}^{N-1} [z((n+1)T_s) - z(nT_s)]^2$$

$$\hat{c}_z(0) := \frac{1}{N} \sum_{n=0}^{N-1} z^2(nT_s) - \left(\frac{1}{N} \sum_{n=0}^{N-1} z(nT_s) \right)^2$$

and C is a constant depending on T_s, and whether $z(t) = \mathcal{R}\{h(t)\}$, $|h(t)|^2$, or $H(t)$. We should briefly mention that Anim-Appiah has analyzed ω_D^{HS} in a recent paper [48], where he considered the cases $z(t) = |h(t)|^n$ and $z(t) = \mathcal{R}\{h(t)\}^n + \mathcal{I}\{h(t)\}^n$, where n is a positive integer.

In order to justify the term 'covariance-based' for Equation (27), we should mention that $E[V(T_s)] = 2[c_z(0) - c_z(T_s)]$ depends on the covariance of $z(t)$. Austin and Stüber have shown that Reference [29]:

$$\lim_{T_s \to 0} \frac{1}{T_s} \sqrt{\frac{E[V(T_s)]}{c_z(0)}} = \sqrt{\frac{-c_z''(0)}{c_z(0)}} \qquad (28)$$

which, under the assumption of isotropic scattering and no LOS component, can be shown to be $\sqrt{2}\omega_D$ when $z(t) = \mathcal{R}\{h(t)\}$, or ω_D when $z(t) = |h(t)|^2$. The limit in Equation (28) can be derived by substituting $2[c_z(0) - c_z(T_s)]$ for $E[V(T_s)]$, moving the $1/T_s$ inside the square root, and applying L'Hôspital's rule twice. The expression in Equation (28) is useful because it facilitates analysis of the covariance-based estimators for small T_s and large N when $\boldsymbol{\psi} \neq \mathbf{0}$, with the same techniques used for the LCR and the ZCR estimators because all of these estimators ultimately depend on $[-c_z''(0)/c_z(0)]^{1/2}$.

An interesting fact that has not been pointed out in the literature is that the limit in Equation (28) does not exist when $z(t) = H(t)$ and $K = 0$ because $c_H''(0)$ is not finite, as can be verified from Equation (16). Having the envelope-squared process $|h(t)|^2$ with a finite $c_{|h|^2}''(0)$, which after a logarithmic transformation $10\log(\cdot)$ yields a process $H(t)$ for which $c_H''(0)$ does not exist, seems counter-intuitive, but could actually have been predicted from Bello's work [52]. It was shown in Reference [52] that the RMS Doppler spread of a Gaussian process $h(t)$ (which is proportional to $c_h''(0)$) and the RMS Doppler spread of $\mathcal{K}(|h(t)|^2)$ are related by a scale constant that does not depend on the Doppler spectrum of $h(t)$, but only on the memoryless nonlinearity $\mathcal{K}(\cdot)$. It turns out that when $\mathcal{K}(\cdot) = 10\log(\cdot)$, the integral expression for the scale factor in Reference [52] does not converge, which is in agreement with our finding that the limit in Equation (28) does not exist when $z(t) = H(t)$. The practical impact of this result is that whenever $z(t) = H(t)$ is used in Equation (27), as was done in Reference [18], the dependence of C on T_s is going to be very strong for small T_s, which might cause problems in the accuracy of the estimator. Moreover, when $z(t) = H(t)$, the effect of $\boldsymbol{\psi} \neq \mathbf{0}$ is not as conveniently characterized through $c_z''(0)$ and $c_z(0)$ by

assuming a small T_s, as it is when $z(t) = \mathcal{R}\{h(t)\}$ or $z(t) = |h(t)|^2$, which we pursue next.

Using the expressions for $r_x^{(n)}(0)$, $n = 0, 1, 2$ in Equations (8)–(10), we show that when T_s is small and N is large, Equation (27) is scaled as a function of K, κ, α and θ_0, and derive the corresponding scale function $A_z(\boldsymbol{\psi})$. Consider first the case $z(t) = \mathcal{R}\{h(t)\}$. Using Equations (2), (8) and (10) we obtain:

$$\begin{aligned}\sqrt{\frac{-2c_z''(0)}{c_z(0)}} &= \sqrt{\frac{-2r_h''(0)}{r_h(0)}} \\ &= \omega_D \left[\frac{1}{(K+1)}\left(1+\frac{\cos(2\alpha)I_2(\kappa)}{I_0(\kappa)}\right)\right. \\ &\quad \left.+\frac{K}{K+1}(1+\cos(2\theta_0))\right]^{\frac{1}{2}} \\ &:= \omega_D A_{\mathcal{R}\{h\}}(\boldsymbol{\psi}) \end{aligned} \tag{29}$$

The first equality in Equation (29) is obtained by using the fact that $c_{\mathcal{R}\{h\}}^{(n)}(0) = r_h^{(n)}(0)/2$, $n = 0, 2$, whenever $\mathcal{R}\{h(t)\}$ has zero mean, which holds if we assume that ϕ_0 in Equation (3) is a uniformly distributed random variable. Notice that $A_{\mathcal{R}\{h\}}(\mathbf{0}) = 1$ as expected. Examining Equation (29) more closely, we realize that for large values of K, the scale factor is not influenced by κ and α, and depends solely on the LOS direction θ_0. An extreme case would be $\theta_0 = \pi/2$ for large K, which would yield a Doppler estimate of $\hat{\omega}_D = 0$. This is because $h(t)$ in Equation (3) would not be time-dependent, a situation where the received signal contains no information about ω_D.

To derive the effect of $\boldsymbol{\psi}$ on covariance-based estimators that use $|h(t)|^2$, we recall Equation (28). Using Equation (14) to calculate the right-hand side of Equation (28), we see that the estimator gets scaled by a factor of $A_{|h|^2}(\boldsymbol{\psi})$, where:

$$\begin{aligned} &A_{|h|^2}(\boldsymbol{\psi}) \\ &= \left[\frac{\left(1+\dfrac{\cos(2\alpha)I_2(\kappa)}{I_0(\kappa)}\right) - 2\left(\dfrac{\cos(\alpha)I_1(\kappa)}{I_0(\kappa)}\right)^2}{\begin{array}{c}+K\left(2+\dfrac{\cos(2\alpha)I_2(\kappa)}{I_0(\kappa)}+\cos(2\theta_0)\right.\\ \left.-4\cos\theta_0\dfrac{\cos(\alpha)I_1(\kappa)}{I_0(\kappa)}\right)\end{array}}{1+2K}\right]^{\frac{1}{2}} \end{aligned} \tag{30}$$

Observe that the scale factor $A_{|h|^2}(\mathbf{0}) = 1$. Note also that for $\kappa = \alpha = 0$, Equation (30) reduces to $A_{|h|^2}(K, \theta_0, 0, 0) = [1 + K\cos(2\theta_0)/(1+2K)]^{1/2}$, which is a result derived in Reference [18] for uniform AOA, later generalized to Equation (30) in Reference [13].

In Figures 13 and 14, we plotted $A_{\mathcal{R}\{h\}}(\boldsymbol{\psi})$ and $A_{|h|^2}(\boldsymbol{\psi})$ versus K and κ for $\theta_0 = \alpha = 0$ and $\theta_0 = \alpha = \pi/2$. We observe that in Figure 13, $A_{\mathcal{R}\{h\}}(\boldsymbol{\psi})$ behaves very similarly to $A_{\mathrm{ZCR}}(\boldsymbol{\psi})$ in Figure 12, which is not surprising since the ZCR estimator and the covariance-based estimator when $z(t) = \mathcal{R}\{h(t)\}$ both converge to the same value for large N and $K = 0$. In Figure 14, we observe that κ has a strong influence on $A_{|h|^2}(\boldsymbol{\psi})$, especially when $\theta_0 = \alpha = 0$.

The effect of additive, zero-mean Gaussian noise $n(t)$ with a two-sided spectral density and a finite spectral support on Equation (27) has been characterized in Reference [18], where $z(t) = |h(t) + n(t)|^2$.

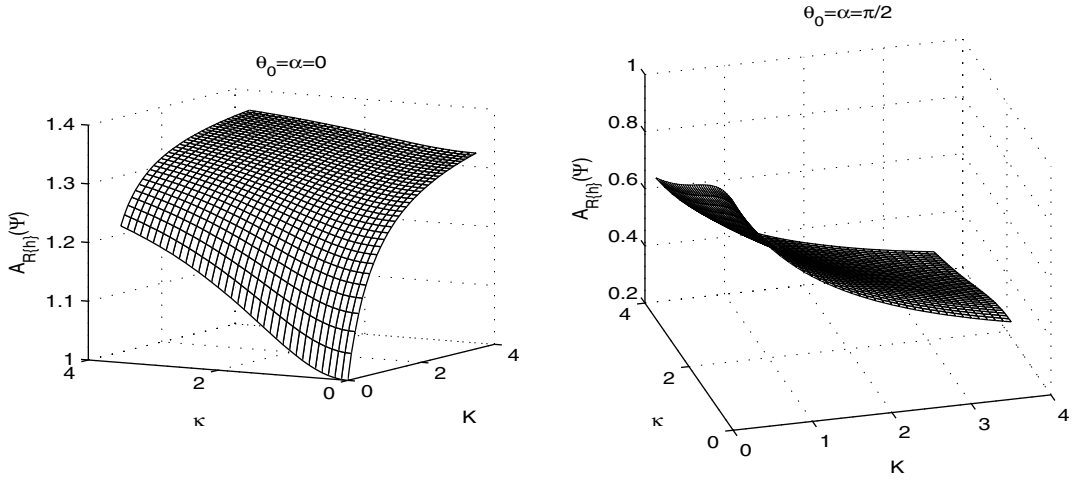

Fig. 13. $A_{\mathcal{R}\{h\}}(\boldsymbol{\psi})$ in Equation (29) versus κ and K.

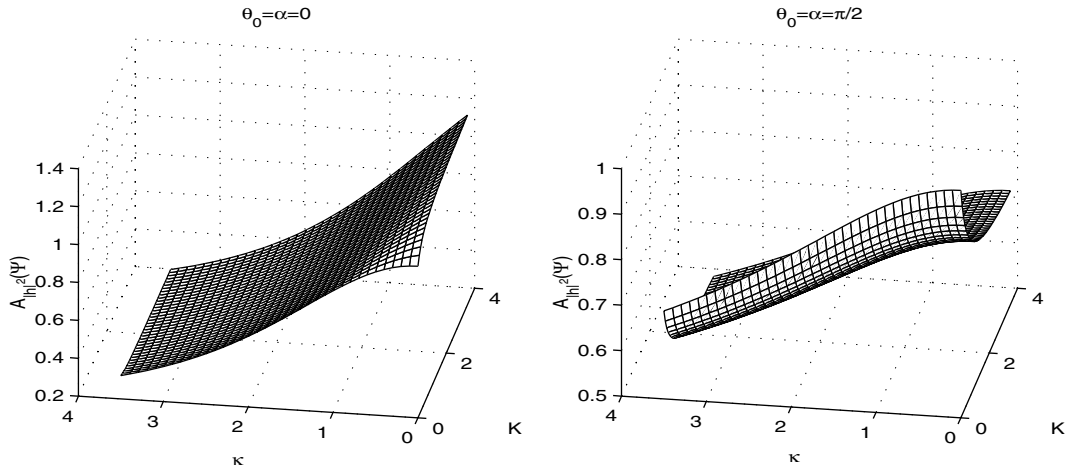

Fig. 14. $A_{|h|^2}(\boldsymbol{\psi})$ in Equation (29) versus κ and K.

It was shown that the noise introduces a bias that increases with the noise bandwidth until it saturates at a certain value. This saturation value, in turn, increases with decreasing T_s. In fact, it is argued in Reference [18] that for a fixed SNR, as the noise gets more and more uncorrelated (with increasing noise bandwidth), with smaller and smaller T_s, the bias grows without bound.

In what follows, we discuss the effect of additive *white* noise that is assumed to be independent of $h(t)$, on Equation (27) when $z(t) = \mathcal{R}\{h(t) + n(t)\}$. The assumption of uncorrelated noise samples holds where $\hat{\omega}_D^{HS}$ in Equation (27) is calculated using noisy channel samples obtained with pilot sequences. With the cascade of the transmit and receive filters designed to have Nyquist properties to avoid intersymbol interference, the channel estimates are corrupted by uncorrelated noise in discrete time.

For large N, Equation (27) is given by,

$$\hat{\omega}_D^{HS} \approx \frac{C}{T_s}\sqrt{\frac{2[c_z(0) - c_z(T_s)]}{c_z(0)}} \tag{31}$$

which, using the independence of $h(kT_s)$ and $n(kT_s)$, and the fact that $c_{\mathcal{R}\{h\}}^{(n)}(0) = r_h^{(n)}(0)/2$, $n = 0, 2$, as was mentioned right after Equation (29), can be written as:

$$\hat{\omega}_D^{HS} \approx C\sqrt{\frac{\mathcal{R}\{r_h(0) - r_h(T_s)\}}{T_s^2[r_h(0) + r_n(0)]} + \frac{2r_n(0)}{T_s^2[r_h(0) + r_n(0)]}} \tag{32}$$

where we used the fact that $r_n(kT_s) = 0$ for $n \neq 0$. But we know that since T_s is small, we can use Equation (28) to obtain:

$$\hat{\omega}_D^{HS} \approx C\sqrt{\frac{-r_h''(0)}{[r_h(0) + r_n(0)]} + \frac{2r_n(0)}{T_s^2[r_h(0) + r_n(0)]}} \tag{33}$$

We see that if the SNR $:= r_h(0)/r_n(0)$ is moderate/low, with T_s being very small, the second term in Equation (33) causes $\hat{\omega}_D$ to deviate from ω_D in a pronounced manner owing to the presence of noise ($r_n(0) \neq 0$). So, similar to the case $z(t) = |h(t) + n(t)|^2$, investigated in Reference [18], when $z(t) = \mathcal{R}\{h(t) + n(t)\}$, uncorrelated noise samples $n(kT_s)$ cause the estimator bias to grow without bound as the sampling duration goes to zero.

One way to overcome this limitation is to avoid $r_n(0)$ by adopting the following variation on $\hat{\omega}_D^{HS}$ in Equation (27):

$$\begin{aligned}\hat{\omega}_D &= \frac{1}{T_s}\sqrt{-\frac{2}{3}\frac{[V(T_s) - V(2T_s)]}{\hat{r}_z(0)}} \\ &\approx \sqrt{-\frac{2}{3}\frac{\mathcal{R}\{r_h(2T_s) - r_h(T_s)\}}{T_s^2[r_h(0) + r_n(0)]}}\end{aligned} \tag{34}$$

for large N. When T_s is small, Equation (34) yields $[-2r_h''(0)/(r_h(0) + r_n(0))]^{1/2}$, which like Equation (33) is also influenced by $r_n(0)$, but not nearly as much because for moderate SNRs, the denominator $r_h(0) + r_n(0) \approx r_h(0)$, so $\hat{\omega}_D$ does not deviate from ω_D significantly. A similar 'denoising' approach was suggested in Reference [29] for robustness against cochannel interference.

Another approach recently proposed in References [13] and [50] motivated by Equation (28) has sought to estimate $c_z''(0)$ and $c_z(0)$ separately. Estimation of $c_z''(0)$ and $c_z(0)$ is done by fitting a parabola to the L points of the sample covariances $\{\hat{c}_z(lT_s)\}_{l=0}^{L}$, and assuming that the sampling rate $1/T_s$ is sufficiently high to insure $LT_s \ll 1$. This condition is satisfied, for example, if channel samples used to estimate $c_z(0)$ and $c_z''(0)$ are provided by channel estimators of narrowband TDMA systems, similar to Reference [40]. The steps for the approach in Reference [13] are as follows:

Step 1: Find the covariance estimates $\{\hat{c}_z(lT_s)\}_{l=0}^{L}$ by sample averaging;
Step 2: Find $\hat{a}_n = \text{argmin}_{a_n} \sum_{l=0}^{L} |\hat{c}_z(lT_s) - \sum_{n=0}^{2} a_n l^n|^2$, $n = 0, 2$;
Step 3: Obtain $\hat{c}_z^{(n)}(0) = n!\hat{a}_n/T_s^n$, $n = 0, 2$;
Step 4: Substitute $\hat{c}_z^{(n)}(0)$, $n = 0, 2$, in Equation (28), and use the corresponding C depending on whether $z(t) = \mathcal{R}\{h(t)\}$ or $z(t) = |h(t)|^2$.

Note that the mapping from the covariance estimates to the derivative estimates that solves the least squares problem in Step 2 ($\{\hat{c}_z(lT_s)\}_{l=0}^{L} \rightarrow \{\hat{c}_z^{(n)}(0)\}_{n=0}^{2}$) is a linear transformation (a $3 \times (L+1)$ matrix multiplication) which can be precomputed once T_s is known. Unlike Reference [40], the method described in Steps 1–4 only uses a second-order polynomial to estimate ω_D, which obviates unnecessary approximations and the need for finding the roots of a higher than second-order polynomial.

The approach in Reference [13] facilitates a natural obviation of the effect of uncorrelated noise when $z(t) = \mathcal{R}\{h(t)\}$. To circumvent the effect of uncorrelated noise in this case, Reference [13] performs the minimization in Step 2 by not using the zeroth lag $\hat{c}_z(0)$, which is most affected by the presence of white noise. When the data record is large enough, this approach is unaffected by the SNR, and as we show later, it even outperforms the 'denoised' estimator in Equation (34).

We should note that the analysis that led to Equations (29) and (30) also holds for the estimator in Reference [13], since, like Reference [18], it approximates Equation (28) when T_s is small and N is large. An issue that remained unaddressed so far, which has not received much attention in the literature is the performance of velocity estimators when the data record is finite. An expression for the variance of the number of zero crossings of a narrowband Gaussian process (corresponding to $K = 0$) can be found in Reference [53] (p. 212). A simpler formula that is a special case of this result for processes with symmetric spectra (corresponding to $\boldsymbol{\psi} = \mathbf{0}$) is reported in References [54] and [55] (p. 85). However, not many results are available for the variance of envelope LCR estimators for finite data records. Also, even though the mean squared consistency of a class of covariance-based estimators is proved in Reference [13], variance expressions for when the data record is finite is not available in the literature. Hence, we resort to simulations in the next section to compare the velocity estimators' performance when the data record is finite.

4.3. Effect of Finite Data Record

Since the effect of $\boldsymbol{\psi} \neq \mathbf{0}$ was characterized analytically, we assume $\boldsymbol{\psi} = \mathbf{0}$ in this subsection. In our simulations, we generated 100 different realizations of $h(t)$ using the simulator in Reference [56] which approximates Clarke's spectrum, and for the given method, plotted the histogram for the 100 velocity estimates normalized by the true velocity, corresponding to each realization. The performance of each estimator can be judged by how closely its histogram is clustered around 1. In all experiments $v = 100$ km h^{-1}, and $T_s = 4.12 \times 10^{-5}$, which is the symbol period for the IS-54 TDMA standard adopted in North America. The carrier frequency is $f_c = 900$ MHz implying $\omega_D/2\pi \approx 83.3$ Hz. For the method in Reference [13] we chose $L = 15$ correlation lags.

In Figure 15 we observe that for a time duration of 20 ms ($N = 485$ samples) the sample variances of the covariance-based estimators ($\hat{\omega}_D^{HS}$ in Equation (27) and the one proposed in Reference [13]) are an order of magnitude smaller than their LCR-based counterpart, and that the estimator in Reference [13] has a slightly smaller sample variance than $\hat{\omega}_D^{HS}$. This illustrates that as far as convergence of estimators to their ensemble values is concerned, at high sampling rates and small estimation windows, covariance-based estimators are more reliable than their LCR-based counterparts. This is because, for such small data lengths, the signal does not experience many level crossings as can also be seen from the top-left plot in Figure 15. This large gap in the maximum Doppler spread estimator variance for small window lengths between the LCR-based schemes and those that rely on the covariances, have recently been reported in Reference [13], and is important to know in contexts where quick estimates of ω_D are needed, such as adaptive modulation/coding.

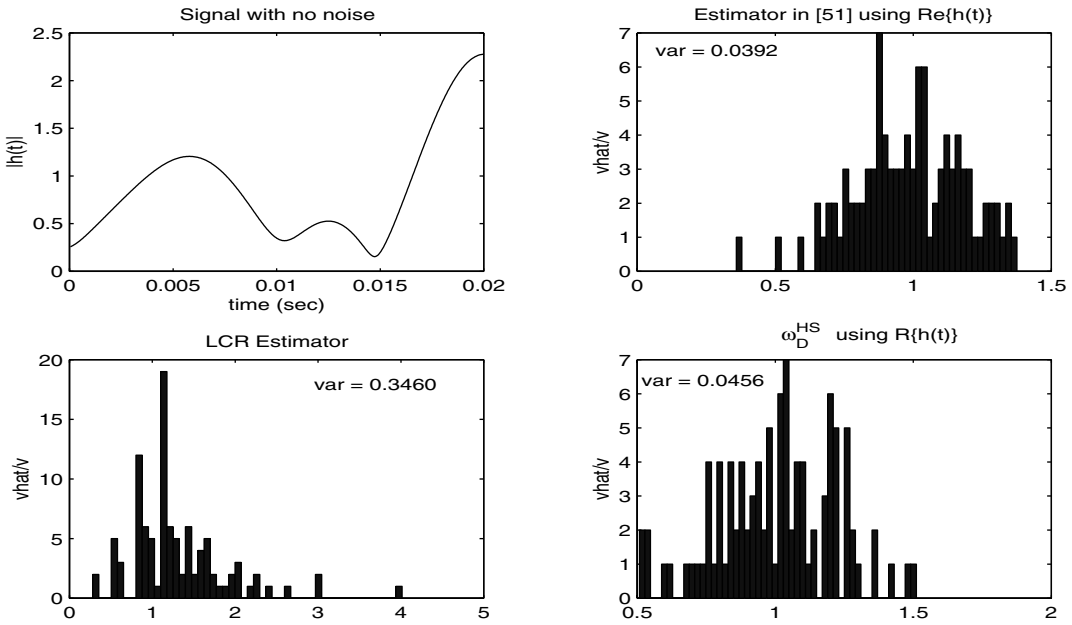

Fig. 15. Histogram of velocity estimates for $N = 485$ ($NT_s = 0.02$ s).

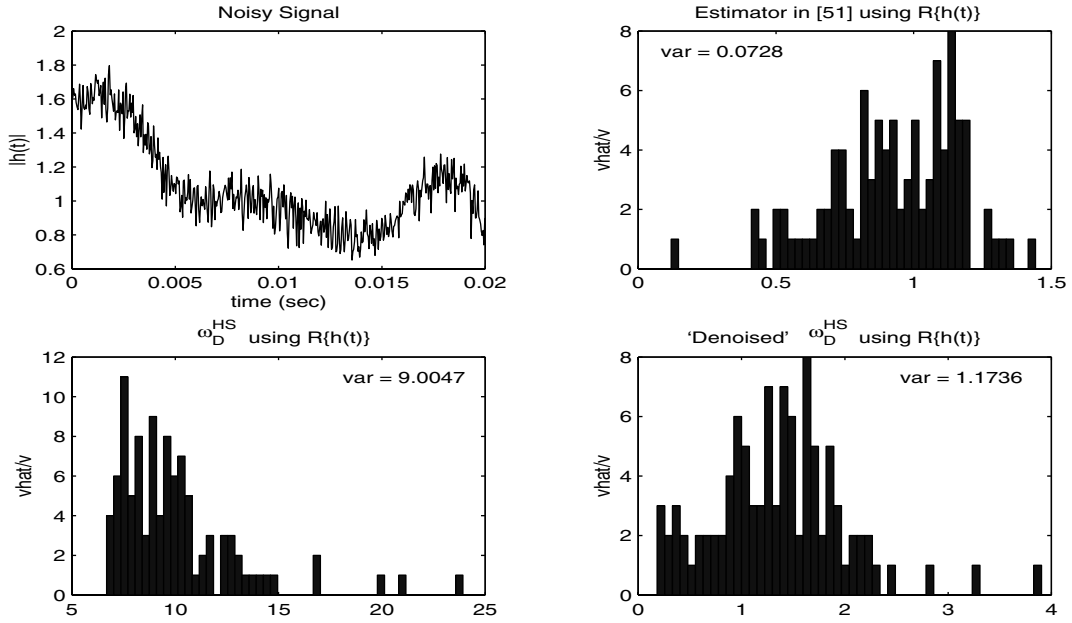

Fig. 16. Histogram of velocity estimates for $N = 485$, SNR $= 20$ dB.

In Figure 16 we look at the effect of white noise at SNR $= 20$ dB. We observe that $\hat{\omega}_D^{HS}$ performs very poorly as explained by Equation (33). The estimator in Reference [13] obtained by avoiding the zeroth covariance lag $\hat{c}_{\mathcal{R}\{h\}}(0)$ has an order of magnitude less variance than the one obtained by 'denoising' $\hat{\omega}_D^{HS}$, given in Equation (34), in the presence of noise.

In conclusion, we see that as far as the convergence of sample estimates and sensitivity to white noise is concerned, the estimator in Reference [13] is always the best alternative, when $T_s \ll 1$. The intuitive explanation for this is that the estimator in Reference [13] involves more correlation lags and hence it is more reliable as compared to $\hat{\omega}_D^{HS}$. Naturally, utilizing more correlation lags to improve

performance comes at the expense of more computational complexity.

5. Conclusion

In this paper, we summarized the current state of the art in signal strength estimation, velocity estimation, and estimation of related channel parameters which are influential in system performance. In our discussion of signal strength estimation, we gave emphasis to the pioneering works in References [14, 29–31] and illustrated the effects of LOS, nonisotropic scattering and sampling rate as well as shadow correlation distance and shadow variance on the estimator performance. Then we discussed Doppler-based velocity estimation under the umbrella of LCR-based estimators and covariance-based estimators. We characterized the effects of model imperfections owing to the presence of LOS, nonisotropic scattering and additive noise on many of the velocity estimators, utilizing a unifying framework and illustrated the effect of finite data length via simulation.

References

1. Pollini G. Trends in handover design. *IEEE Communications Magazine*, 1996; **34**(3): 82–90.
2. Stüber GL. *Principles of Mobile Communication*. Kluwer Academic Publishers, 1996.
3. Vijayan R, Holtzman JM. A model for analyzing handoff algorithms. *IEEE Transactions on Vehicular Technology*, 1993; **42**(3): 351–356.
4. Chu MJ, Stark WE. Effect of mobile velocity on communications in fading channels. *IEEE Transactions on Vehicular Technology* 2000; **49**(1): 202–210.
5. Duel-Hallen A, Hu S, Hallen H. Long-range prediction of fading signals. *IEEE Signal Processing Magazine*, 2000; **17**(3): 62–75.
6. Bello PA. Some techniques for the instantaneous real-time measurement of multipath and Doppler spread. *IEEE Transactions on Communication Technology* 1965; **13**(3): 285–292.
7. Tepedelenlioğlu C, Giannakis GB. Precoding for scattering function estimation of mobile channels using output correlations only. *Proceedings of the 37th Allerton Conference on Communication, Control and Computing* 1999.
8. Aulin T. A modified model for the fading signal at a mobile radio channel. *IEEE Transactions on Vehicular Technology*, 1979; **28**: 182–203.
9. Pätzold M, Killat U, Laue F. An extended Suzuki model for land mobile satellite channels and its statistical properties. *IEEE Transaction on Vehicular Technology* 1998; **47**(2): 617–630.
10. Jakes WC. *Microwave Mobile Communications*. IEEE Press: New York, 1974.
11. Mardia KV. *Statistics of Directional Data*. Academic Press, 1972.
12. Abdi A, Barger HA, Kaveh M. A parametric model for the distribution of the angle of arrival and the associated correlation function and power spectrum at the mobile station. *IEEE Transactions on Vehicular Technology*, September 1999, submitted.
13. Tepedelenlioğlu C, Giannakis GB. On velocity estimation and correlation properties of narrowband communication channels. *IEEE Transactions on Vehicular Technology*. Submitted.
14. Goldsmith AJ, Greenstein LJ, Foschini GJ. Error statistics of real-time power measurements in cellular channels with multipath and shadowing. *IEEE Transactions on Vehicular Technology* 1994; **43**(3): 439–446.
15. Wong D, Cox DC. Estimating local mean signal power level in a Rayleigh fading environment. *IEEE Transactions on Vehicular Technology* 1999; **48**(3): 956–959.
16. Chockalingam A, Dietrich P, Milstein L, Rao R. Performance of closed-loop power control in DS-CDMA cellular systems. *IEEE Transactions on Vehicular Technology* 1998; **47**(3): 774–789.
17. Hata M, Nagatsu T. Mobile location using signal strength measurements in a cellular system. *IEEE Transactions on Vehicular Technology* 1980; **VT29**(2): 245–252.
18. Holtzman JM, Sampath A. Adaptive averaging methodology for handoffs in cellular systems. *IEEE Transactions on Vehicular Technology*, 1995; **44**(1): 59–66.
19. Gudmundson M. Correlation model for shadow fading in mobile radio systems. *Electronics Letters* 1991; **27**(23): 2145–2146.
20. Mockford S, Turkmani AMD, Parsons JD. Local mean signal variability in rural areas at 900 MHz. *Proceedings of the 40th Vehicular Technology Conference*, 1990; 610–615.
21. Giancristofaro D. Correlation model for shadow fading in mobile radio channels. *Electronics Letters* 1996; **32**(11): 958–959.
22. Austin MD, Stüber GL. In service signal quality estimation for TDMA cellular systems. *Proceedings of the Vehicular Technology Conference* 1996; 1155–1159.
23. Andersin M, Mandayam N, Yates R. Subspace based estimation of the signal to interference ratio for TDMA cellular systems. *Proceedings of the IEEE 46th Vehicular Technology Conference* 1996; **2**: 1155–1159.
24. Türkboyları M, Stüber GL. An efficient algorithm for estimating the signal-to-interference ratio in TDMA cellular systems. *IEEE Transactions on Communications* 1998; **46**(6): 728–731.
25. Balachandran K, Kadaba S, Nanda S. Channel quality estimation and rate adaptation for cellular mobile radio. *IEEE Journal on Selected Areas in Communications* 1999; **17**(7): 1244–1256.
26. Beaulieu NC, Toms AS, Pauluzzi DR. Comparison of four SNR estimators for QPSK Modulations. *IEEE Communications Letters*, 2000; **4**(2): 43–45.
27. Dassanayake P. Dynamic adjustment of propagation dependent parameters in handover algorithms. *Proceedings of the 44th Vehicular Technology Conference* 1994; **1**: 73–76.
28. Sampath A, Holtzman JM. Adaptive handoffs through the estimation of fading parameters. *Proceedings of the International Conference on Communications* 1994; **2**: 1131–1135.
29. Austin MD, Stüber GL. Velocity adaptive handoff algorithms for microcellular systems. *IEEE Transactions on Vehicular Technology* 1994; **43**(3): 549–561.
30. Lee WCY, Yeh YS. On the estimation of the second-order statistics of lognormal fading in mobile radio environment. *IEEE Transactions on Communications*, 1974; **COM22**(6): 869–873.
31. Lee WCY. Estimate of local average power of a mobile radio signal. *IEEE Transactions on Vehicular Technology* 1985; **VT34**(1): 22–27.
32. Santucci F, Huang W, Bhargava V. A framework for analyzing the user membership in cellular CDMA networks. *IEEE Transactions on Communications* 2000; **48**(3): 442–454.
33. Narasimhan R, Cox DC. Estimation of the nonstationary mean signal in wireless systems using wavelets. *Proceedings*

of Global Telecommunications Conference (GLOBECOM) 432–436.
34. Valenzuela RA, Landron O, Jacob DL. Estimating local mean signal strength of indoor multipath propagation. *IEEE Transactions on Vehicular Technology*, 1997; **46**(1): 203–212.
35. Greenwood D, Hanzo L. Characterization of mobile radio channels. *Mobile Radio Communications*. Pentech: London, 1992; 163–185.
36. Greenstein LJ, Michelson DG, Erceg V. Moment–method estimation of the Ricean *K*-factor. *IEEE Communication Letters* 1999; **3**(6): 175–176.
37. Prakash R, Veeravalli V. Adaptive hard handoff algorithms. *Proceedings of the 49th Vehicular Technology Conference* 1999;**3**: 1779–1783.
38. Lu J, Xu X, Zou H, Greenleaf J. Application of Bessel beam for Doppler velocity estimation. *IEEE Transactions on Ultrasonics Ferroelectrics & Frequency Control*, 1995; **42**(4): 649–662.
39. Ehrman L, Esposito R. On the accuracy of the envelope method for the measurement of Doppler spread. *IEEE Transactions on Communication Technology* 1969; 578–581.
40. Lin J, Proakis JG. A parametric method for Doppler spectrum estimation in mobile radio channels. *Proceedings of the 27th Conference on Information Systems and Sciences (CISS '93)* 1993; John Hopkins University, Baltimore, MD: 875–880.
41. Austin MD, Stüber GL. Eigen-based Doppler estimation for differentially coherent CPM. *IEEE Transactions on Vehicular Technology* 1994; **43**(3): 781–785.
42. Kawabata K, Nakamura T, Fukuda E. Estimating velocity using diversity reception. *Proceedings of the 44th Vehicular Technology Conference* 1994; **1**: 371–374.
43. Doumi TL, Gardiner JG. Use of base station antenna diversity for mobile speed estimation. *Electronics Letters* 1994; **30**(22): 1835–1836.
44. Blostein SD, Liu Y. A change-detection approach to monitoring fading channel bandwidth. *Proceedings of IEEE International Symposium on Information Theory, Whistler, B.C., Canada*, 1995; 155.
45. Abdi A. Kaveh M. A new velocity estimator for cellular systems based on higher order crossings. *Proceedings of the 32nd Asilomar Conference on Signals Systems and Computers*, 1998; 1423–1427.
46. Hansen H, Affes S, Mermelstein P. A Rayleigh Doppler frequency estimator derived from maximum likelihood theory. *Proceedings of the 2nd IEEE Workshop on Signal Processing Advances in Wireless Communications (SPAWC '99)* 1999; 382–386.
47. Mottier D, Castelain D. A Doppler estimation for UMTS-FDD based on channel power statistics. *Proceedings of the* 49th *IEEE Vehicular Conference* 3052–3056
48. Anim-Appiah KD. On generalized covariance-based velocity estimation. *IEEE Transactions on Vehicular Technology* 1999; **48**(5): 1546–1557.
49. Narasimhan R, Cox DC. Speed estimation in wireless systems using wavelets. *IEEE Transactions on Communications* 1999; **47**(9): 1357–1364.
50. Tepedelenlioğlu C, Giannakis GB. A spectral moment approach to velocity estimation in mobile communications. *Proceedings of the WCNC 2000*. To appear.
51. Abdi A. Higher-order-crossing-based velocity estimation in cellular systems. *Wireless Communication Systems Course Project Report*. Department of Electrical and Computer Engineering, University of Minnesota, Minneapolis, MN, 1998.
52. Bello PA. On the RMS bandwidth of nonlinearly envelope detected narrowband Gaussian noise. *IEEE Transactions on Information Theory* 1965; **IT11**: 236–239.
53. Cramér H, Leadbetter MR. *Stationary and Related Stochastic Processes*. John Wiley & Sons: Chichester, 1967.
54. Blachman NM. Narrowband Gaussian noise: variance of the number of zero crossings. *Electronics Letters* 1978; 75–76.
55. Blachman NM. *Noise and its effect on communication*. Robert E. Krieger Publishing Company, 1982.
56. Höher P. A statistical discrete-time model for the WSSUS multipath channel. *IEEE Transactions on Vehicular Technology*, 1992; **41**(4): 461–468.

Authors' Biographies

Cihan Tepedelenlioğlu was born in Ankara, Turkey in 1973. He received his B.S. degree with highest honors from the Florida Institute of Technology in 1995, and his M.S. degree from the University of Virginia in 1998, both in electrical engineering. Since January 1999 he has been working as a research assistant at the University of Minnesota, and is currently a Ph.D. student in the Department of Electrical and Computer Engineering.

His research interests include statistical signal processing, system identification, time-varying systems, and modeling, tracking, and equalization of fading channels in mobile communications.

Ali Abdi is a Ph.D. candidate in the Department of Electrical and Computer Engineering, University of Minnesota, Minneapolis. His previous research interests have included stochastic processes, wireless communications, pattern recognition, neural networks, and time series analysis. His current work is mainly focused on different aspects of wireless communications, with special emphasis on channel modeling, antenna arrays, and system performance evaluation.

Georgios B. Giannakis received his Diploma in Electrical Engineering from the National Technical University of Athens, Greece in 1981. From September 1982 to July 1986 he was with the University of Southern California (USC), where he received his MSc. in Electrical Engineering, (1983), MSc. in Mathematics (1986), and Ph.D. in Electrical Engineering, (1986).

After lecturing for one year at USC, he joined the University of Virginia (UVA) in 1987, where he became a professor of Electrical Engineering in 1997, Graduate Committee Chair, and Director of the Communications, Controls, and Signal Processing Laboratory in 1998. He was awarded the School of Engineering and Applied Science Junior Faculty Research Award (UVA) in 1988, and the UVA-EE Outstanding Faculty Teaching Award in 1992. Since January 1999 he has been with the University of Minnesota as a professor of Electrical and Computer Engineering.

His general interests lie in the areas of signal processing and communications, estimation and detection theory, time-series analysis, and system identification–subjects on which he has published more than 100 journal papers. Specific areas of expertise have included (poly)spectral analysis, wavelets, cyclostationary, and non-Gaussian signal processing with applications to sensor array and image processing. Current research focuses on transmitter and receiver diversity techniques for equalization of single- and multi-user communication channels, mitigation of rapidly fading wireless channels, compensation of nonlinear amplifier effects, redundant filterbank transceivers for block transmissions, multicarrier, and wide-band communication systems.

G. B. Giannakis received the IEEE Signal Processing Society's 1992 Paper Award in the Statistical Signal and Array Processing (SSAP) area, and co-authored the 1999 Best Paper Award by Young Author (M. K. Tsatsanis). He co-organized the 1993 IEEE Signal Processing Workshop on Higher-Order Statistics, the 1996 IEEE Workshop on Statistical Signal and Array Processing, and the first IEEE Signal Processing Workshop on Wireless Communications in 1997. He guest (co-)edited two special issues on high-order statistics (*International Journal of Adaptive Control and Signal Processing*, and the EURASIP journal *Signal Processing*), and the January 1997 special issue on signal processing for advanced communications (*IEEE Transactions on Signal Processing*). He has served as an Associate Editor for the *IEEE Transactions on Signal Processing* and the *IEEE Signal Processing Letters*, a secretary of the Signal Processing Conference Board, a member of the SP Publications board and a member and vice-chair of the SSAP Technical Committee. He now chairs the Signal Processing for Communications Technical Committee and serves as the Editor in Chief for the IEEE Signal Processing Letters. He is an IEEE Fellow, a member of the IEEE Fellow Election Committee and also a member of the European Association for Signal Processing.

Mostafa Kaveh received the BS and PhD degrees in Electrical Engineering from Purdue in 1969 and 1974 respectively and the MS degree from UC Berkeley in 1970. He has been at the University of Minnesota since 1975 where he is presently a professor and Head of the Department of Electrical and Computer Engineering.

Dr. Kaveh is a Fellow of IEEE, was a former member of the Board of Governors and a past Vice President for Publications of the IEEE Signal Processing Society and was the General Chairman of ICASSP93. He received the 1986 ASSP Society Senior (best paper) Award (with A. Barabell), the 1988 ASSP Society Meritorious Service Award, and an IEEE Third Millennium Medal in 2000.